Advanced Over-the-Horizon Radar

MITRE

Advanced Over-the-Horizon Radar

C. Callan
J. Cornwall
P. Diamond
S. Drell
D. Eardley
S. Flatté
G. MacDonald
C. Max
F. Perkins
A. Peterson
J. Sullivan
J. Vesecky

JSR-90-105

February 1993

JASON
The MITRE Corporation
7525 Colshire Drive
McLean, Virginia 22102-3481
(703) 883-6997

REPORT DOCUMENTATION PAGE

Form Approved
OMB No. 0704-0188

1. AGENCY USE ONLY (Leave blank)	2. REPORT DATE	3. REPORT TYPE AND DATES COVERED
	February 11, 1993	

4. TITLE AND SUBTITLE
Advanced Over-The-Horizon Radar

5. FUNDING NUMBERS
PR - 8503A

6. AUTHOR(S)
C. Max et al.

7. PERFORMING ORGANIZATION NAME(S) AND ADDRESS(ES)
The MITRE Corporation
JASON Program Office A020
7525 Colshire Drive
McLean, VA 22102

8. PERFORMING ORGANIZATION REPORT NUMBER
JSR-90-105

9. SPONSORING/MONITORING AGENCY NAME(S) AND ADDRESS(ES)
DARPA/TIO
3701 North Fairfax Drive
Arlington, Virginia 22203-1714

10. SPONSORING/MONITORING AGENCY REPORT NUMBER
JSR-90-105

11. SUPPLEMENTARY NOTES

12a. DISTRIBUTION/AVAILABILITY STATEMENT
WARNING: This document contains technical data whose export is restricted by the Arms Export Control Act (Title 23, U.S.C., Sec 2751, et seq. or the Export Administration Act of 1979, as amended, Title 50, U.S.C., Appl. 2401 et seq. Variations of these export laws are subject to severe criminal penalties. Dissemunate in accordance with provision of DoD Directive 5320.25.

12b. DISTRIBUTION CODE

13. ABSTRACT (Maximum 200 words)

In the summer of 1990, JASON conducted a study on Advanced Over-the-Horizon (AOTH) radar. The task of the study was to evaluate DARPA's plans and roles for a proposed experimental test bed (FTB) facility, which would be a precursor to an eventual operational AOTH system. The goal of both the AOTH and the ETB systems was improved detection of individual cruise missiles attacking the continential United. States.

14. SUBJECT TERMS
meteors, self-focusing, HF noise, side-lobe powers, ionosphere radar in clutter research, WARF

15. NUMBER OF PAGES

16. PRICE CODE

17. SECURITY CLASSIFICATION OF REPORT	18. SECURITY CLASSIFICATION OF THIS PAGE	19. SECURITY CLASSIFICATION OF ABSTRACT	20. LIMITATION OF ABSTRACT
UNCLASSIFIED	UNCLASSIFIED	UNCLASSIFIED	SAR

Contents

PREFACE: Update as of August 1992

In the summer of 1990, JASON conducted a study on Advanced Over-the-Horizon (AOTH) radar. The task of the study was to evaluate DARPA's plans and roles for a proposed experimental test bed (ETB) facility, which would be a precursor to an eventual operational AOTH system. The goal of both the AOTH and the ETB systems was improved detection of individual cruise missiles attacking the continental United States.

The report that follows, originally drafted in the summer and fall of 1990, contains the results of the JASON summer study. The report outlines the issues affecting AOTH radar performance, highlights the critical areas needing resolution, and suggests generic types of experiments on existing facilities that could help evaluate the effect of these critical issues on AOTH performance. It points out, however, that a coherent, ongoing research program would be needed in order to attain this goal, and states that an oversight group for these experiments would be very desirable for the successful execution of the suggested research program.

The JASON summer study report also points out that Over-the-Horizon (OTH) radar is a tool that has a variety of interesting missions besides cruise-missile detection. These include detection of aircraft (both military and illicit drug-trade related), improved detection of ships in a variety of sea-states, applications to arms control monitoring and treaty verification, and intelligence missions. What these missions have in common is the need for a ground-based system with wide surveillance capabilities.

The results of the 1990 JASON summer study were circulated broadly within DARPA in draft form. However, in view of the substantial delay

between the draft JASON report and the publication of this final version, we thought it would be worthwhile to discuss what has come to pass subsequent to the 1990 summer study.

Events since the 1990 summer study fall into two categories: a second DARPA-sponsored study, and the vastly changed international political context.

The LCAS Study

In January 1991, DARPA commissioned the Low Cost Alternative Study (LCAS), tasked to investigate less expensive alternatives to the proposed experimental test bed for OTH. The stated goal remained the development of a capability to detect individual cruise missiles as they attacked the continental United States. But in view of a more constrained budget situation, the LCAS panel was asked to develop lower-cost alternatives to the ETB, and to make recommendations for experiments on other facilities which could help to evaluate the feasibility of the AOTH radar system.

The JASON AOTH summer study, which was discussed with the LCAS panel, had recommended strongly that DARPA develop an experimental plan for resolving the main issues affecting AOTH performance. The LCAS report Ref. [P-1] put forward just such a specific plan, for experiments that could be done on existing facilities.

In our view this plan represents a major step forward. The LCAS panel developed its plan via careful analysis of the "experimental logic" needed to characterize the different types of clutter affecting AOTH performance, as well as to resolve the companion issues of ionospheric coherence limitations,

side-lobe performance, and ionospheric absorption. The LCAS panel concluded that existing facilities such as the ROTHR radar in Virginia, in conjunction with enhanced instrumentation and smaller auxiliary radars, could address the principal issues that need to be settled before the performance of an AOTH radar can be confidently predicted. It recommended a dedicated experimental program lasting three to five years. We would, however, place higher priority than LCAS on ionospheric heating effects. Voice-of-America facilities can be used to investigate these issues, but an Air Force internally funded program at the Geophysics Laboratory has been terminated.

The LCAS report reinforced two important conclusions of the JASON summer study:

It recommended that DARPA provide "enduring guidance and leadership" for the OTH radar program. In addition, it said that there "should be an independent and objective review group to advise DARPA" as the experimental program evolves.

In terms of a broader context for the AOTH program, the LCAS report pointed out that OTH radar has "substantial promise in a number of applications: intelligence, fleet defense, battlefield defense and targeting, continental air defense, drug interdiction, and cueing other systems with limited surveillance capability."

The Changed Political Context

The disintegration of the Soviet Union and the Eastern Bloc have created a vastly different political context since the time of the JASON and LCAS studies. In particular, the prospect of a coordinated sneak-attack on

the continental United States by Soviet cruise missiles now seems far more remote. Yet this was the main mission for AOTH development. What are the implications for over-the-horizon radar technology if that original mission now looks much less imminent?

One consequence is clearly a budgetary one: it is even less likely than it was two years ago that hundreds of millions of dollars will be available for a dedicated experimental test bed for over-the-horizon radar. Thus if any experiments are to be done at all, they will have to be of the type recommended by the LCAS panel, using existing or slightly modified OTH facilities as much as possible. The LCAS panel felt that experiments of this type could be of great assistance in determining the potentials and risks of an advanced OTH system.

A second consequence of the changed political context is that DARPA must reassess the benefits and costs of an advanced OTH technology development program. If the original threat of a coordinated Soviet cruise-missile attack on the continental United States has dwindled, are there still strong motivations for pursuing advanced OTH capabilities?

It seems to us that there are applications of OTH that remain compelling. They would be particularly compelling if the original performance goal of using OTH to detect individual cruise-missile-sized objects (or objects with similar radar cross sections) can be achieved.

The OTH applications that seem to us to be worth evaluating take advantage of the fact that OTH is one of only a few ground-based technologies having wide surveillance capability. Therefore it is important to evaluate the potential effectiveness of OTH against aircraft in a theater military applica-

tion or in a counter-narcotics role; for detection of ships in a fleet defense role; for arms control monitoring and treaty verification; and for several interesting intelligence missions. If OTH technology proves sufficiently capable, several of these roles have high leverage. For example, surveillance of third-world missile test ranges to determine operating characteristics, especially the existence and timing of possible submunition releases, would be a capability of high value in planning our next generation of defense against theater ballistic missiles.

The above roles for OTH are diverse, and fall under the bureaucratic purviews of several different government agencies and services, both military and civilian. Thus it seems to us that DARPA is a natural place for advanced technology development in this area to continue.

REFERENCE

P-1. Lynn, L., J. Allen, M. Balser, D. Briggs, J.D. Carlos, J. Freedman, J. Gobien, R. Leadabrand, A. Peterson, and S. Spoerri, "AOTH ETB Low Cost Alternative Study (LCAS)," report prepared by Atlantic Aerospace Electronics Corporation and published by Rome Laboratory, Air Force Systems Command (October 1991).

EXECUTIVE SUMMARY

The development of over-the-horizon (OTH) radar systems for reliable detection of cruise missiles and other targets with small radar cross sections is a very ambitious task. Success will require the ability to lower the level of spread-doppler clutter by several orders of magnitude from the values seen on OTH radar systems today. The fact that cruise missiles are already visible under some circumstances on existing OTH systems gives one hope that this can be accomplished. Nevertheless, at night when the OTH radar frequency is low and the cruise-missile radar cross section is therefore very small, detection will require substantial improvement over current capabilities.

The DARPA program for developing an advanced over-the-horizon (AOTH) radar seeks to minimize spread-doppler clutter by several approaches; use of: 1) a radar beam that is narrow in both the vertical and cross-beam directions, to reduce signals arriving on unwanted propagation paths; 2) low side-lobe levels, to reduce spurious signals such as those from auroral regions; and 3) good range resolution (accomplished via high bandwidth), to eliminate backscattering from meteor trails and other ionospheric irregularities near the desired OTH propagation path. In addition, there are plans to reduce noise from discrete sources, such as lightning, by adaptive beamforming.

At present it is clear that the most limiting issues for the success of AOTH radars for cruise-missile detection involve ionospheric phenomena of natural origin, rather than issues primarily of systems design and antenna engineering. As a consequence, we are convinced that improving the capabilities of OTH against cruise missiles will require an *ongoing research program* in factors affecting OTH radar propagation. This ongoing research program will need greater emphasis on continuity, and more scientific oversight, than

has been typical of many previous military development programs.

Since most of the relevant natural phenomena are ionospheric, about which a considerable amount is already known, an ongoing AOTH research program will require better coupling to the extensive research communities that already exist in the fields of ionospheric and magnetospheric physics, wave propagation through random media, and ionospheric modification.

The proposed experimental test bed (ETB) facility needs to be viewed as one step in an active, ongoing AOTH research program. The architecture and design of the ETB will be best arrived at in a context in which one is addressing the specific phenomena affecting OTH sensitivity, both experimentally and theoretically. A strong start in this direction can be made by studying what can be learned using existing data from facilities such as the wide aperture radar facility (WARF), Jindalee, Cobra Mist, etc., and by doing further experiments with existing facilities, perhaps with modest modifications. Although the DARPA program plan for AOTH shows that existing facilities are being used for this purpose at present, the plan presented during the course of this study [summer 1990] indicates that these experiments are scheduled to be discontinued in the near future. We are convinced that discontinuing these experiments with existing facilities would be a mistake, and we thus recommend that they be continued and strengthened. For example, a series of experiments specifically focused on understanding the role of meteor trails in creating spread-doppler clutter could contribute much understanding by exploiting existing equipment at various locations around the world.

The design and siting of a new ETB facility should take into account the fact that a variety of missions for OTH radar will need to be studied

over the lifetime of the ETB facility. Cruise missiles are clearly an important target for any OTH research program. Other tasks of national importance for which OTH research data are crucial are: the limits of OTH radar for the detection of large- and medium-sized aircraft under a realistic variety of environmental conditions (whether the aircraft are cruise-missile carriers or are carrying illicit drugs into the United States); the possibility of improved detection of ships of all sizes in various sea states; possible applications to the verification of arms control agreements; and specialized intelligence missions. Other important applications will surely arise in the future. The design of the ETB must be *flexible* enough to accommodate meaningful experiments associated with a variety of potential missions.

The optimal siting of the ETB facility needs to keep in mind a spectrum of potential missions and users, as well as the fundamental technical issues that need to be explored in a multi-year program to determine the limits of OTH radar performance. In particular, the ETB needs to be sited so that it can view targets over land as well as sea. It needs to be able to view at least one area where the United States does test flights of ALCMs and SLCMs. The facility should be positioned to view areas that have substantial commercial and military air traffic, ship traffic, and train and truck traffic. The possibility of cooperative experiments using existing ionospheric diagnostic facilities such as incoherent-scatter radars should also be considered in the siting decision for the ETB.

We examine in this study several physical effects which could be causes of spread-doppler clutter, the limiting factor in OTH performance. These effects include meteor trails, round-the-world propagation and multipath effects, random phase perturbations, and self-focusing instabilities that could potentially be driven by the high power of the AOTH system itself. We also

examine atmospheric noise characteristics, and present some preliminary recommendations for experiments to evaluate the importance and scaling of the various propagation effects.

Considering the long-range issues that are important to AOTH development, we recommend that a broadened AOTH research program should have ongoing scientific oversight, preferably by an interdisciplinary group. The oversight group or advisory committee should represent not only the radar community, but also ionospheric and magnetospheric physicists, specialists in wave propagation in random media, and in ionospheric modification. The AOTH program should also include representatives of potential mission applications other than cruise-missile detection. The AOTH program should be focused on the long-range needs of OTH research for the country.

1 INTRODUCTION

Over-the-horizon (OTH) radars achieve longer ranges than line-of-sight radars by utilizing reflection from the ionosphere. Radar frequencies in the HF band, 3 to 30 MHz, are low enough to be reflected by the ionosphere, yet high enough not to experience prohibitive amounts of absorption there. Since the electron density in the ionosphere increases due to photoionization during the day, the higher HF radar frequencies can be used during daylight hours. At night, when the ionospheric electron density is low, one is constrained to frequencies below 10-15 MHz.

Because of its long range (hundreds to thousands of km) and its wide-area surveillance capabilities, over-the-horizon radar is a potentially powerful tool for a variety of military missions. Two of these missions have already been chosen as the basis for deployed OTH systems: detection and tracking of aircraft offshore of the continental United States (the OTH-B system, operated by the Air Force), and detection and tracking of aircraft and ships that are potential threats to U.S. battle groups (the ROTHR system, operated by the Navy).

Future missions for OTH radar systems are important as well. These include reliable detection and tracking of cruise missiles, drug interdiction, and a variety of potential OTH applications for treaty monitoring and verification.

The present report concentrates on the application of OTH radar to detect cruise missiles. A previous JASON report [Reference 1-1] contains an overview of the issues involved in the use of over-the-horizon radar for

early warning of cruise missile attack. In the present report we will focus on developments since 1987, and on current plans for an experimental test bed (ETB) facility.

OTH radars use doppler shift measurements to differentiate between returns from moving targets and those from the ground or sea. Hence any phenomena that introduce doppler shifts into the signal contribute what is called "spread-doppler clutter;" this can mask moving targets with small cross sections. One of the main goals of an advanced OTH radar system would be to minimize such unwanted doppler returns.

There are three principal approaches to minimizing spread-doppler clutter: 1) The radar should have narrow beams in both the vertical (elevation) and cross-beam (azimuthal) directions to reduce signals arriving on unwanted propagation paths. Existing OTH radars have wide vertical beams so that simultaneous reception on several rays is possible. Narrow beams also help reduce the size of the resolution cell, so the signal from the target is larger relative to the backscatter from the surrounding sea or ground. 2) Sidelobe levels should be kept very low, to reduce spurious signals such as those from auroral regions, where scattering from moving ionization irregularities introduces doppler shifts. 3) Judicious use of range resolution (via high bandwidth), together with good azimuthal and elevation resolution, would eliminate scattering from meteor trails and other ionospheric irregularities near the desired OTH propagation path.

The proposed ETB facility would demonstrate whether incorporating the above principles into an OTH radar system will yield appreciable reduction in the spread-doppler clutter, and hence an improved ability to detect small targets such as cruise missiles.

The use of OTH radar for surveillance, detection, and tracking of cruise missiles poses a major technological challenge. Whereas large aircraft may have radar cross sections of several hundred square meters at 6 MHz, the radar cross section of the current generation of cruise missiles is much smaller than this. Use of low-observable technologies can reduce the radar cross section still further, at relatively low cost. With present OTH systems, highly reliable detection of cruise missiles at all times of day and all environmental conditions is not possible.

Because OTH radar requires ionospheric propagation and reflection, it is sensitive to the state of the ionosphere, which changes with time of day, season, solar activity, auroral activity, and other natural influences. Cruise-missile detection with OTH radar becomes particularly difficult at night when one is forced to use low operating frequencies: the radar cross section falls off sharply once the radar wavelength (30 to 50 meters at night) is larger than the geometric size of the cruise missile. This is the region where the Rayleigh approximation applies, and the radar cross section varies as the minus fourth power of the radar wavelength. Figure 1-1 illustrates this effect.

In what follows, we review the issues affecting OTH radar performance against small targets, discuss the elements needed for an effective research program in AOTH radar, and assess the implications for the mission and architecture of an experimental test bed. The emphasis of Section 2 will be on physics and technology issues that will increase the probability of detection of cruise-missile-scale targets. In Section 3, we discuss how one can learn the most from a future ETB facility. In Section 4, we give simple calculations, which suggest that even advanced OTH radar systems would be expected to encounter difficulties in detecting low-observable cruise missiles. As a consequence, if low-observable technology is implemented on cruise missiles,

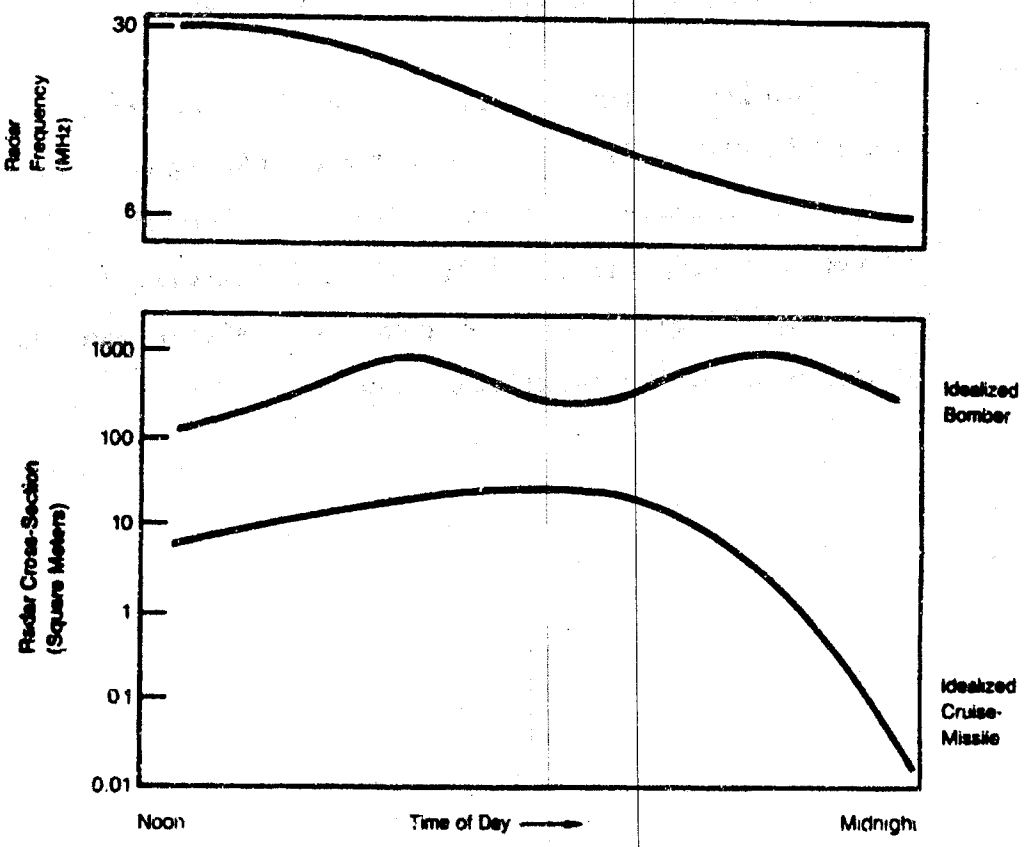

Figure 1-1. Schematic variation of OTH radar frequency and target cross-section with time of day.

an AOTH system operating as part of an overall air defense network would be less than 100% effective, particularly at night and at certain seasons of the year. AOTH still could have an important role to play, however, when viewed as one of a suite of complementary sensors including ground-based and airborne line-of-sight radars, infrared sensors, and other systems.

We would like to thank the people who provided us with briefings on the current DARPA AOTH program, and on issues affecting the status of plans for the experimental test bed: W. Sievers and G. Guttrich (MITRE); R Cormier, A. Gould, P. Franchi, J. Morris, and E. Tichovolsky (RADC); and L. Sweeney (Mirage). We very much appreciate the effort and care which these briefers put into their presentations to us.

REFERENCE

1-1. Banks, P., R. Davis, A. Despain, S. Drell, G. MacDonald, W. Nierenberg, A. Peterson, O. Rothaus, J. Sullivan, J. Vesecky, and F. Zachariasen. *Technical Issues in Early Warning of Cruise Missile Attack (U), JASON Report No. JSR-87-801 (MITRE Corporation, McLean, VA, 1988).*

2 A RESEARCH PROGRAM IN ADVANCED OVER-THE-HORIZON RADAR

2.1 Background and Perspective

The most critical questions in the successful application of OTH to cruise-missile detection appear to involve ionospheric phenomena of natural origin, rather than issues primarily of systems design and antenna engineering. This fact implies that improving OTH capabilities against cruise missiles will require an ongoing research program, rather than a one-time effort to develop a single new facility. This AOTH research program will need more scientific oversight than is usual in typical military development programs. Since most of the relevant natural phenomena involve the ionosphere, about which a considerable amount is already known, the AOTH research program will also require much better coupling to the extensive research communities that have expertise in ionospheric and magnetospheric physics, wave propagation through random media, and ionospheric modification. It is our impression that these communities have not been adequately engaged in the AOTH effort to date — the latter having involved mainly the radar community. Conversely, the ionospheric and magnetospheric physics communities do not appear to be well informed about the contributions they might make to the AOTH problem. A successful AOTH research program needs to take

steps to actively reach out to these researchers, and to engage their expertise in addressing ionospheric problems.

The experimental test bed needs to be viewed as one of many steps in an active, ongoing AOTH research program. The architecture and design of the ETB will be best achieved in a context in which one is addressing specific phenomena affecting OTH sensitivity, both experimentally and theoretically. A strong start in this direction can be made by using existing facilities, perhaps with modest modifications. Although the DARPA program plan for AOTH shows that existing facilities are being used for this purpose at present, the plan also shows that these experiments are scheduled to be discontinued in the near future.

We are convinced that discontinuing these experiments with existing facilities would be a mistake, and recommend that they be continued and strengthened. As we will discuss further below, little direct experimental effort has been put so far into understanding the critical issue of subclutter visibility. We will outline a variety of experiments that can help clarify its origin and amelioration. The results of these experiments can be used directly to design future new facilities.

In the remainder of this section, we discuss several of the most important natural phenomena affecting OTH performance, with the goal of providing the framework for the needed experimental and modeling efforts.

2.2 Propagation Effects and Causes of Spread-Doppler Clutter

2.2.1 Introduction

A variety of different causes for spread-doppler clutter have been suggested, with varying degrees of experimental substantiation. Figure 2-1, illustrates many of these suggested clutter sources.

Some, such as meteor trails and round-the-world ray paths, occur for most OTH radar orientations. Others, such as field-aligned ionospheric irregularties associated with the aurora, occur preferentially for polar OTH ray paths.

A critical task for the ETB will be to isolate these various sources of spread-doppler clutter, in order to determine their scaling and their effect on AOTH performance limits.

2.2.2 Meteors

Reflections from meteor ionization trails may provide the limiting clutter background for high sensitivity OTH radars. Ordinarily the clutter background is set by scattering from the ocean or land surface which result in small doppler shifts. Because of the small shifts, doppler filtering is very effective for separating aircraft or cruise missile target returns from ground- or sea-clutter signals. Meteor trail reflections, on the other hand,

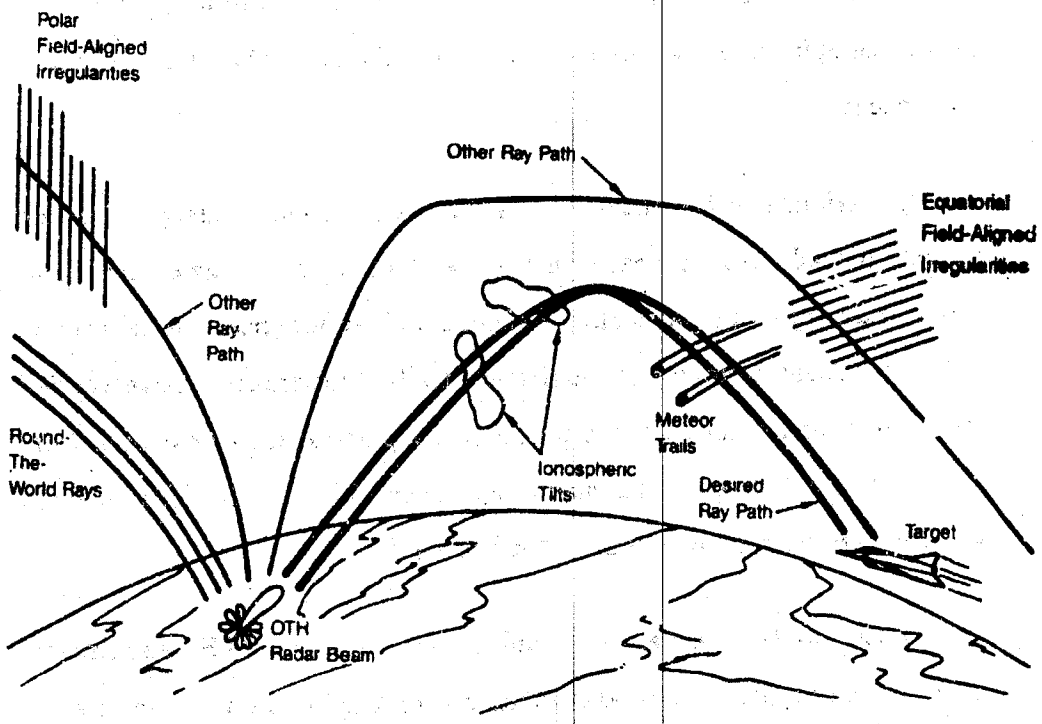

Figure 2-1. Schematic illustration of the sources of spread-doppler clutter for OTH radar. Source: The MITRE Corp.

are doppler shifted by the wind velocity in the upper atmosphere which can exceed 100 m/s. In addition, components of the meteor particle velocities are observed during the ionization trail formation which results in still larger doppler shifts. Thus, if propagation conditions cause meteor echoes to occur at the same time delay as targets, a doppler-shifted clutter background can result. Doppler filtering can reduce but not eliminate this residual clutter component.

An estimate of the radar cross section and number density of meteor ionization trails can be based on the result of research carried out some thirty years ago. In particular, Reference 2-1 summarizes the physics of radar reflections from meteor ionization trails. Experiments have verified the theory for ionization trails produced by particle sizes extending from about 10 g to 10^{-7} g (visual magnitudes from -5.0 to + 15). Radar cross sections vary from greater than 10^4 m^2 to 1 m^2.

Meteor trails have been detected in many existing OTH experiments. Three of the propagation modes which can pick up scattering from meteor trails are illustrated in Figure 2-2. Figure 2-3 shows meteor-trail echo power resulting from backscatter in modes 0, 1, and 2 [Reference 2-2].

Meteoritic particles of sufficient size create ionization columns in the altitude interval between 80 and 120 km. The speeds at which the particles strike the earth's atmosphere vary between limits of about 10 and 75 km/s. Those particles which evaporate before striking the earth follow straight paths and decelerate a negligible amount. Ionization is released in the form of a column, initially very small, which rapidly expands owing to diffusion. The ionized atoms are evaporated meteoric material; relatively few air atoms are ionized. To a first approximation, the maximum electron

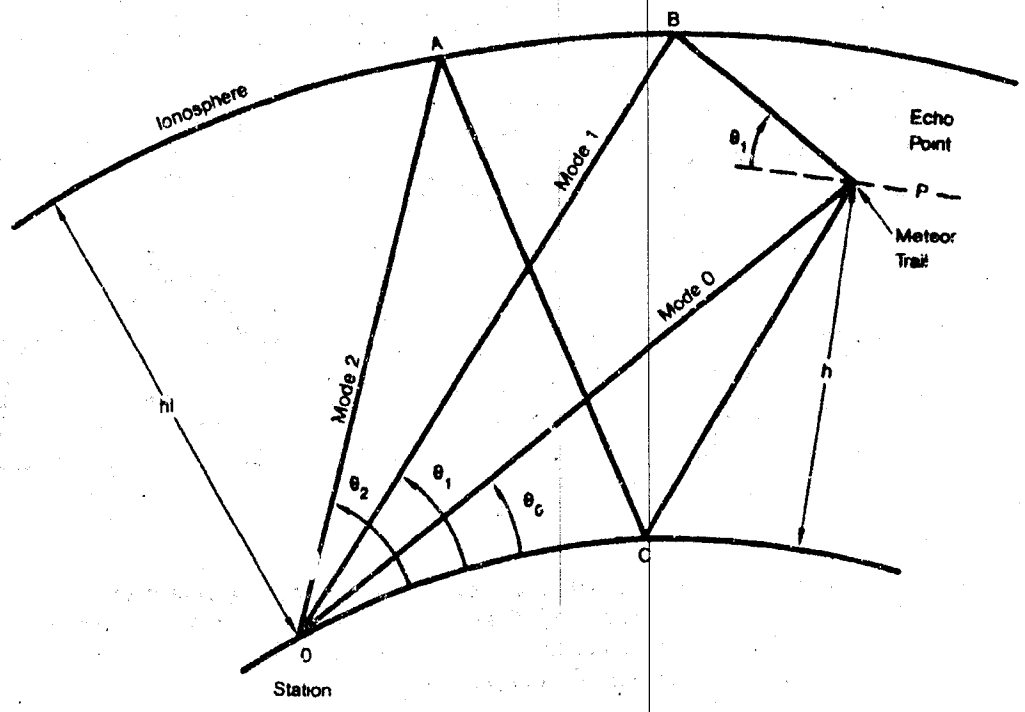

Figure 2-2. Schematic representation of possible meteor echo propagation modes.

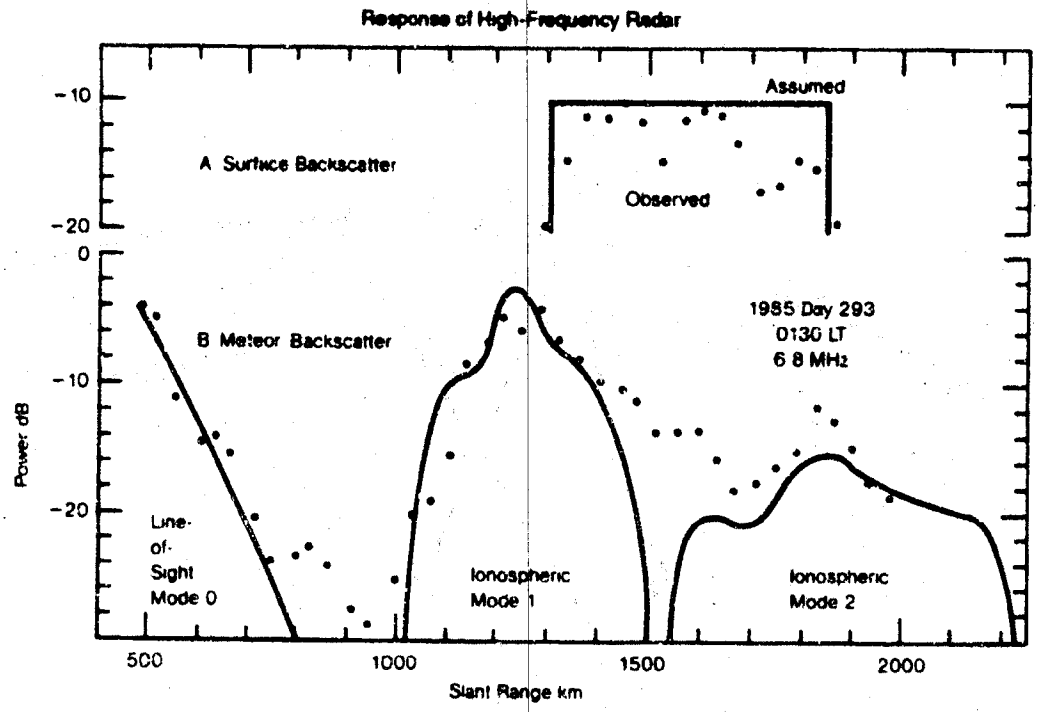

Figure 2-3. Variation with range of effective meteor echo power showing three components which are identifiable with Mode 0, Mode 1, and Mode 2 echoes, defined in figure 2-2. The continuous curve is the prediction. The earth surface clutter return is shown for comparison at the top of this figure. Source: Reference 2-2.

density created per unit length of trail is dependent only on the mass of the particle and the cosine of the zenith angle of its path.

Order-of-magnitude estimates of relationships between particle number, particle mass, visual magnitude, particle size, and line density of ionization produced are listed in Table 2-1, from Reference 2-3, and are illustrated in Figure 2-4.

The radar cross section of underdense meteor trails is given by

$$\sigma = n_e \sigma_e, \qquad (2-1)$$

where $\sigma_e = 0.66 \times 10^{-28}$ m^2 is the Thomson cross section of an electron and n_e is the number of electrons scattering coherently [Reference 2-4]. For underdense trails which are relevant in this discussion

$$n_e = n_L F, \qquad (2-2)$$

where n_L is the electron line density and $F = \sqrt{2R\lambda}$ is the Fresnel length corresponding to the length within which the electrons scatter in phase. For an OTH radar with wavelength $\lambda = 30$ m (frequency $f = 10$ MHz) scattering from a meteor at a range R = 2,000 km, we find $F \simeq 10^4$ m.

From Table 2-1 we observe that ionization from a 10^{-8} g meteor creates an electron line density of 10^9/m, resulting, thereby, from (2-1) and (2-2) in a radar cross section for specular reflection of $\sigma = 0.66 \times 10^{-2}$ m^2 at a range of 2,000 km and with $f = 10$ MHz.

With a cross section of about -22 db, such a meteor, or a more massive one, might be confused with a target if we use a -22 db search threshold. To make a quantitative determination, we calculate the rate at which such meteors occur and how many on the average would appear in the range resolution

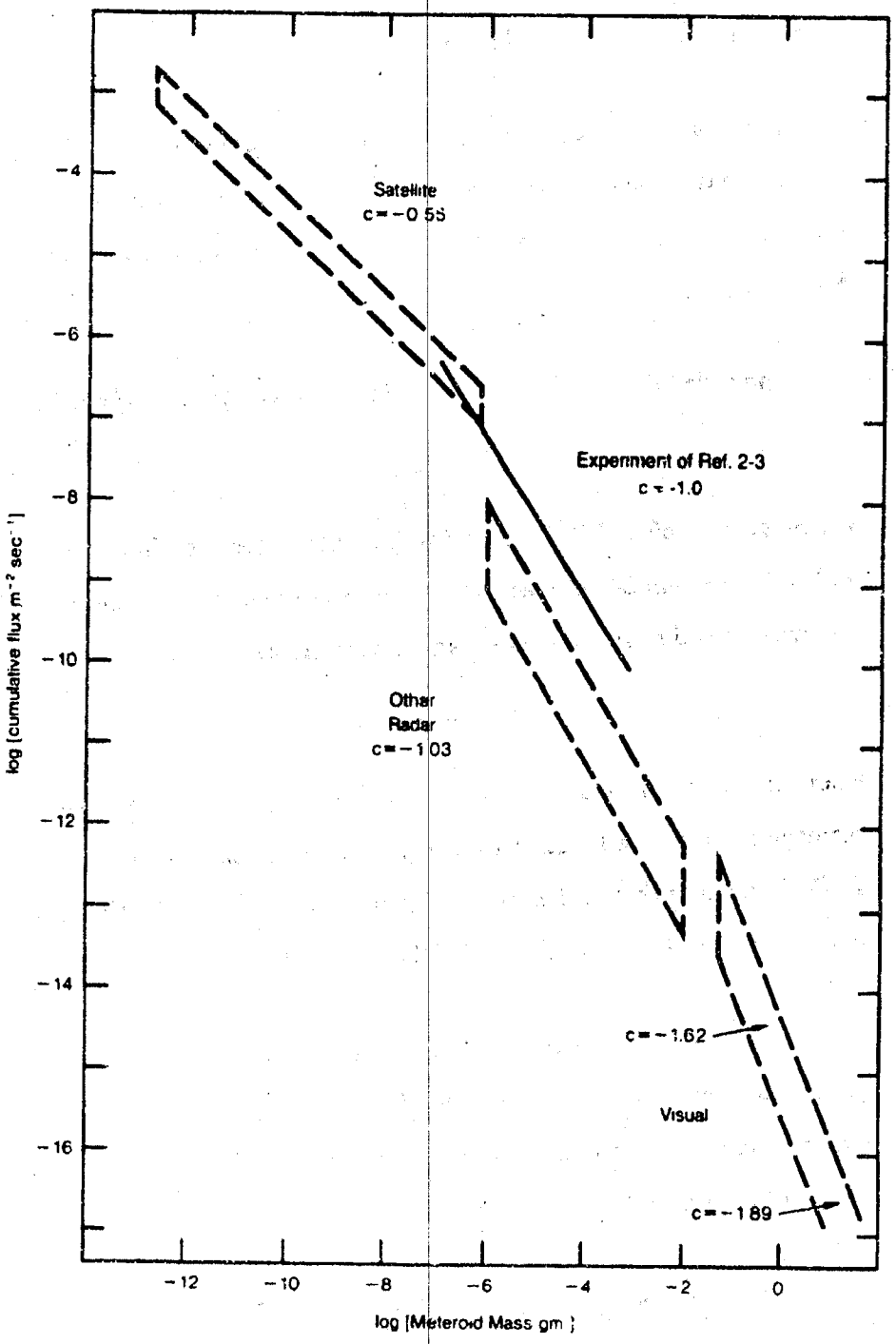

Figure 2-4. The cumulative mass distribution of meteors entering the earth's atmosphere, from Reference 2-3 The exponent (c) of the power law relation between cumulative flux and mass varies from about -0 55 to -1.89

Table 2-1. Sporadic Meteors: order-of-magnitude estimates of their mass, brightness, size, number, and the electron line density in their trails

	Mass (grams)	Visual Magnitude	Radius	Number of this mass or greater swept up by the earth each day	Electron line density (electrons per meter of trail length)	Number/ sec/ km²
Particles pass through the atmosphere and fall to the ground	10^4	−12.5	8 cm	10	—	—
Particles totally disintegrated in the upper atmosphere	10^3	−10.0	4 cm	10^2	—	—
	10^2	− 7.5	2 cm	10^3	—	—
	10	− 5.0	0.8 cm	10^4	10^{16}	—
	1	− 2.5	0.4 cm	10^5	10^{17}	—
	10^{-1}	0.0	0.2 cm	10^6	10^{16}	—
	10^{-2}	2.5	0.08 cm	10^7	10^{15}	—
Approximate limit of radar measurements —	10^{-3}	5.0	0.04 cm	10^8	10^{14}	—
	10^{-4}	7.5	0.02 cm	10^9	10^{13}	10^{-3}
	10^{-5}	10.0	0.008 cm	10^{10}	10^{12}	10^{-2}
?	10^{-6}	12.5	40 microns	10^{11}	10^{11}	10^{-1}
	10^{-7}	15.0	20 microns	10^{12}	10^{10}	1
	10^{-8}	17.5	8 microns	$<10^{13}$	10^9	≤ 10
Micro-meteorites (Particles float down unchanged by atmospheric collisions)	10^{-9}	20.0	4 microns	Total for this group estimated as high as 10^{20}	Practically none	—
	10^{-10}	22.5	2 microns			
	10^{-11}	25.0	0.8 micron			
	10^{-12}	27.5	0.4 micron			
Particles removed from the solar system by radiation pressure	10^{-13}	30	0.2 micron	—	—	

cell of the AOTH. Assume a horizontal aperture of $a = 10$ km for the prototype AOTH and an effective elevation aperture of $a\ 10 \sin\theta$. The elevation angle θ_1, as illustrated in Figure 2-5, is determined by $\tan\theta_1 = h/(D/2)$, where $h \simeq 300$ km is the effective altitude of the reflecting ionospheric F layer and D is the ground range to target. We then obtain Table 2-2 for the horizontal and elevation angular widths and for the area of the illuminated cell, $D^2\delta\theta_H\delta\theta_{El}$ for a range of operating parameters.

The effective area for ground clutter return is much smaller because of the short pulse length of $1\mu s$ that the AOTH can achieve, corresponding to a range spread of 1/2 (300 m) = 150 m, or an area ranging from $\sim 3/4$ km^2 to 4 km^2 for the range of λ and D considered above. Table 2-1 shows that meteors with masses $\gtrsim 10^{-8}$ g that contribute radar cross sections of $\gtrsim$ -22 dB at distances of 2,000 km and wave lengths $\sim$ 30 m, arrive at the rate of about 10 km$^{-2}s^{-1}$. As to returns from meteors within the same time resolution cell, Figure 2-5 shows that elevation angular spread $\delta\Theta_{El}$ would have to exceed

$$\delta\Theta_{El} = \frac{h_M \sec\Theta_1}{\sqrt{h^2 + (D/2)^2}} \simeq \frac{2h_M}{D} \approx \begin{cases} 5.7°, & \text{D} = 2{,}000 \text{ km} \\ 2.8°, & \text{D} = 7{,}000 \text{ km} \end{cases}$$

for a meteor altitude $h_M \cong 100$ km. This is a significantly larger angular spread than is expected for operation at the diffraction limit except at the longest ranges and largest wavelengths that would be appropriate for nighttime operation.

There are two additional mitigating factors. First, the cross sections calculated from Equations (2-1) and (2-2) are for specular reflection and therefore apply only to that small fraction of meteor tracks moving in a plane perpendicular to the narrow beam of the AOTH. (The doppler shift which OTH relies upon to discriminate target signals from ground clutter will

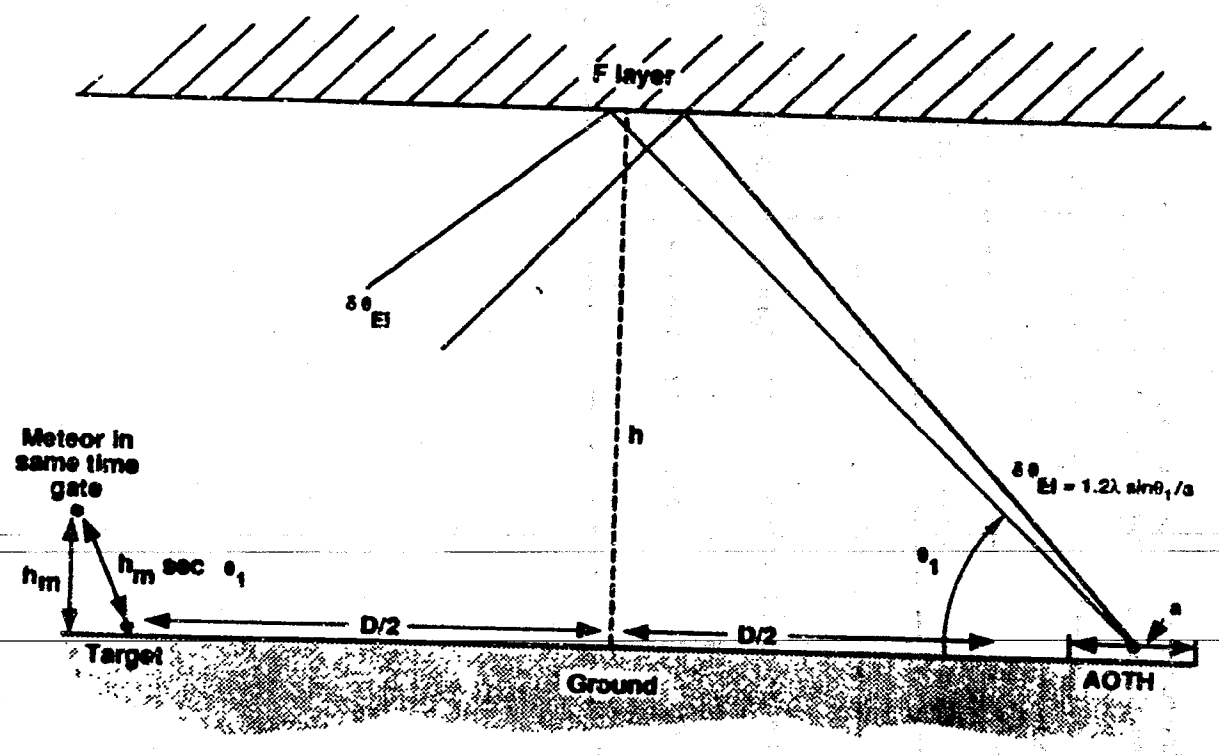

Figure 2-5. Geometry for radar return from meteor trail, within same resolution cell in range.

Table 2-2. The horizontal aperature ($\delta\theta_H$), elevation aperature ($\delta\theta_{EL}$), and illuminated cell area for an AOTH with aperature a = 10 km

λ	f	$\delta\theta_H = 1.2\lambda/a$	$\delta\theta_{EL} = 1.2\lambda \sin\theta_1/a$		Area of Illuminated Cell	
			D = 2000 km	D = 4000 km	D = 2000 km	D = 4000 km
20 m	15 MHz	0.14° = 2.5x10⁻³ rad	0.5° = 8.8x10⁻³ rad	1° = 1.8x10⁻² rad	80 km²	720 km²
30 m	10 MHz	0.21° = 3.7x10⁻³ rad	0.7° = 1.2x10⁻² rad	1.5° = 2.5x10⁻² rad	200 km²	1800 km²
50 m	6 MHz	0.34° = 6x10⁻³ rad	1.1° = 1.9x10⁻² rad	2.2° = 3.5x10⁻² rad	480 km²	3700 km²

arise from the wind velocities in the upper atmosphere, which will generally be cross range relative to meteor tracks.) This will reduce the number of meteors seen by roughly 10^{-2} corresponding to a radar beam width of $\lesssim 1°$ relative to the roughly 50° opening angle of the cone within which meteors enter the atmosphere.

The second important factor that can be used to discriminate against tracks of such small meteors is the fact that they are very short lived, diffusing in a second or less (see Reference 2-2). It should therefore be possible to remove them by requiring multiple radar returns over an approximate 10 s period in order to define a track.

We conclude that *main lobe* viewing of relatively frequent tracks formed by small meteors of mass $\gtrsim 10^{-8}$ g with cross sections $\gtrsim$ -22 dB should not present a problem to AOTH. However there remains a serious question of what radar returns will be seen in the *side lobes*. To answer this question will require a measurement program. Side lobe returns will come from all directions and thus from an area restricted neither by the beam width nor by the condition of specular reflection. Therefore the effective viewing area will be larger within a time resolution cell by as much as

$$\left(\frac{2\pi}{10^{-2}\text{rad}}\right) \cdot 10^2 \sim 10^4 \text{ to } 10^5. \qquad (2-3)$$

Assuming 40 db suppression of side lobe radiation, we must consider meteors of mass $\gtrsim 10^{-6}$ g that create electron line densities $\gtrsim 10^{11}$ electrons/m and by Equation (2-2) radar cross sections 10^4 times larger than 10^{-8} g meteors. These 10^{-6} g meteors occur only at a rate reduced by 10^{-2}, but side lobe returns come from a much larger area, increased by Equation (2-3). It remains to establish experimentally how well, in practice, they can

be discriminated against by the requirement of multiple radar hits for track definition, and by taking advantage of the short 1 s lifetimes of these tracks.

2.2.3 Round-the-World Propagation and Spread-Doppler Clutter

Propagation of HF signals around the world and back to the transmitting site has been known from the early days of HF radio communications [Reference 2-5]. However, little quantitative work has appeared in the literature besides that of Fenwick and Villard at Stanford [References 2-6 and 2-7], and some satellite experiments by Barker and Grossi [Reference 2-8]. Round-the-world (RTW) propagation is observed to have a signal attenuation of the order of 10 dB per trip around the world. Since the front-to-back ratio for the large antennas used in OTH radars is usually less than 10 dB, we can then expect to have transmitted signals arriving at the receiver with significant intensity and an approximate time delay of (140 N ms), N being the number of RTW circuits. Thus, there is a possibility that RTW signals from an OTH radar could interfere with normal operation in the sense of producing unwanted clutter. This possibility has been recognized for some time, but little quantitative research has been done on the topic. We think that RTW signals may well be a factor in the generation of spread-doppler clutter, particularly the "inner" doppler clutter at less than 5 Hz.

To understand the basics of RTW generated clutter consider a radar "echo" arriving with a very long time delay, say 140 ms. If the radar has a sufficiently low pulse repetition frequency (PRF), e.g., less than about 7 Hz, such an echo would be resolved. However, PRFs are usually in the 10 to 100 Hz range and multiple-trip RTW signals would not be resolved, even by a

PRF of 7 Hz. So we are likely to have a RTW radar echo aliased to some range which depends on the exact PRF in use.

This would not be hard to cope with if RTW had a precise time delay and zero doppler shift. However, RTW signals have been shown by Fenwick and Villard [Reference 2-7] to be dispersed in time. They are also known to be spread in doppler shift. The dispersion is important because it spreads the echo power over a number of range bins. For example, a dispersion of 1 ms corresponds to a spread in radar range of about 150 km. Dispersions of the order of 1 ms were noted at 10 to 20 MHz by Fenwick and Villard [Reference 2-7]. RTW measurements at the SRI International wide aperture radar facility (WARF) have indicated doppler spreads of 4 to 5 Hz at levels only 20 dB below the peak signal. The phenomena are complex since OTH radar signals are usually chirp waveforms and the antenna pattern comes into play as well. Nevertheless, the evidence argues strongly that RTW signals can contribute to spread doppler clutter in the inner doppler (< 5 Hz) region.

Given that RTW signals do contribute to spread-doppler clutter, how serious a limitation does this pose for advanced OTH radars? RTW propagation does not occur 100% of the time. The efficiency of RTW propagation changes with geographic location of the radar, operating frequency, azimuth of observation, time of day, season of year, sunspot number, magnetic activity, etc. Reference 2-5 summarizes RTW propagation characteristics. Some salient features are worth pointing out. For example, Fenwick noted, after a year long study [Reference 2-6], that RTW occurs very infrequently outside local daylight hours and most consistently during November and December. A summary of these results is shown in Figure 2-6. RTW propagation has a strong azimuthal dependence. It is most likely to occur for paths that are orthogonal to the line from the radar station to the subsolar point. Many

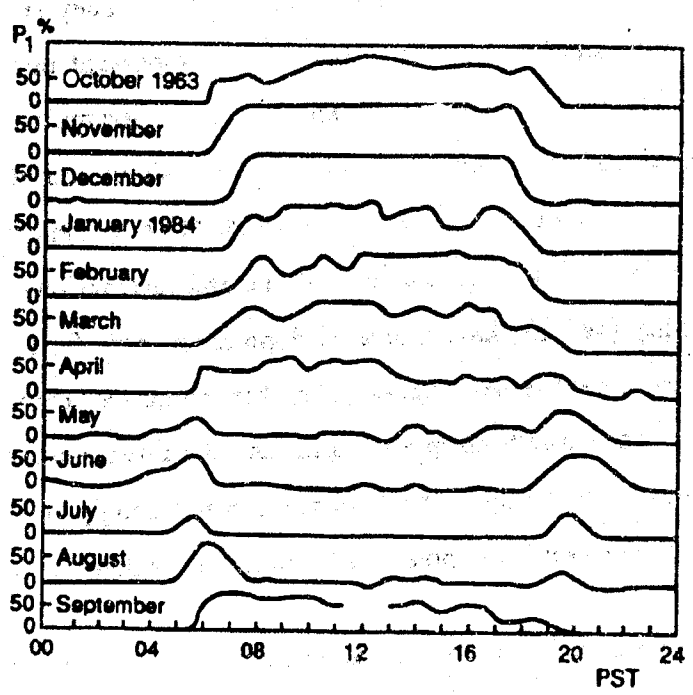

Figure 2-6. Percent occurrence of RTW propagation from Stanford, CA, during the period October 1963 to September 1964. Source: Reference 2-7.

features of RTW propagation, such as the variation with sunspot number, are unknown at this time.

Characteristics such as local time and seasonal variations can be used to do correlation studies relating RTW propagation to the occurrence of spread-doppler clutter. Such studies should help in establishing the role of RTW propagation in the phenomenology of spread-dopper clutter.

If indeed spread-doppler clutter is, in part, due to RTW propagation, then there are ways of mitigating its effect. For example, increasing the front-to-back ratio on the receive and transmit antenna elements should help. Further, we could limit side-lobe radiation in the optimal azimuth direction for RTW propagation.

We have made a zero-order case for the contribution of RTW propagation to spread-doppler clutter. This argument needs to be refined using existing knowledge so that the effects of RTW propagation are better understood, in relation to spread-doppler clutter.

2.2.4 Phase Perturbations

The success of AOTH depends on rejecting clutter in the doppler window of interest. Returns from the earth's surface (land or sea) are usually regarded as contributing to zero-doppler and therefore rejectable. However, the ratio between the clutter at zero-doppler and the clutter in the target doppler window is very large, so a very slight leak into nonzero doppler could swamp the desired signal.

Standard calculations of doppler-shifted clutter involve finite-angle scattering from moving irregularities in the ionosphere. One example would be "orthogonal" scattering from field-aligned irregularities that are in just such a position so that the return is at the correct time to simulate a target and moving in just such a way as to give a reasonable target doppler shift [Reference 2-9]. Another example would replace natural ionospheric irregularities with a meteor trail. A third example is "specular reflection," in which the return path from the ground clutter is not back along the same line as the transmission path, but instead includes a finite-angle (not backscatter) specular reflection from a large-scale ionospheric structure.

Each of these examples predicts different behavior of the signal-to-clutter and noise-to-clutter ratios as a function of range-gated return time and coherent integration time. For example, the "orthogonal scattering" and meteor trail models predict doppler-range relations that are independent of the zero-doppler clutter level at that range, because the path of the EM wave either does not hit the ground, or, if it does, the ground acts as a specular reflector rather than a backscatterer. On the other hand, the "specular reflection" model involves a path for which the energy is nearly backscattered from the same ground that returns the zero-doppler clutter, so the model predicts that the nonzero-doppler level should track with the zero-doppler level; this is in fact observed for an important part of the clutter.

However, another prediction of the "specular reflection" model is that the signal reflecting specularly off a moving ionosphere should be coherent with the return coming directly off the ground (zero-doppler). Observations do not show this. Instead they show that the energy arriving at non-zero doppler shift is mostly incoherent energy (over an integration time of several seconds or more), while the main zero doppler return is coherent over time.

These coherence observations led Franchi and Tichovolsky (Reference 2-10) to put forward a different mechanism for an important part of the nonzero doppler signal. They point out that a moving ionosphere along the transmission path (not backscatter) can make the doppler shift enough to be observed. The effect can occur either on the transmission path or on the return path; presumably it would in fact occur along both. A calculation of the effect requires a model for ionospheric irregularities being swept across the paths, and an integration of the effect along the portions of the paths that pass through the ionosphere. The calculation should be detailed enough to yield both the expected energy as a function of doppler shift, and that energy's dependence on coherent integration time.

Franchi and Tichovolsky present a preliminary calculation in their paper that shows the effect is of the appropriate magnitude. But their calculation was meant only as the beginning step. For convenience in calculations, they modeled the ionospheric irregularities as having a Gaussian spectrum. However, it is known that ionospheric irregularities have power-law spectra, with possibly different power laws in different scale regimes. The integrals in the latter case are harder to do, but must be done to get a quantitative theory. Furthermore, the authors used a crude separation between coherent and incoherent to get estimates. Instead one needs to define and calculate coherence functions of time, so that the results of any integration time can be predicted. Finally, the relationship of results with different antenna sizes, both of the transmitter and of the receiver, needs extensive investigation. In particular, although the case of interest involves backscatter from targets and ground, an investigation of the model could be more efficiently carried out with direct measurements along a one-way path, with a receiver on the ground at a distance at which ground clutter is expected to be generated.

Such experiments are being carried out in relationship to HF communications systems, and their data can be utilized to constrain and categorize the models used for OTH application calculations [Reference 2-11].

2.3 Self-Focusing Instabilities Induced by OTH Radars

One of the unexpected phenomena of high-power ionospheric modification research was the appearance of artificial Spread-F [References 2-12 and 2-13]. This has come to be understood in terms of a self-focusing instability [References 2-14 through 2-16] which creates ionosphere striations deleterious to OTH signal processing. At the simplest level, the instability couples refraction of waves into regions of low-phase velocity (regions of high index of refraction), the heating caused by the corresponding intensity fluctuations, the decrease of plasma density in a hot spot, and the consequent increase of index of refraction n which is related to the plasma density n_e through

$$n^2 = 1 - \frac{\omega_p^2}{\omega^2} = 1 - \frac{4\pi n_e e^2}{m\omega^2}. \qquad (2-4)$$

The question naturally arises: Is the power flux of an OTH radar sufficient to trigger self-focusing instabilities? An unequivocal affirmative answer is given by the experimental results of Novozhilov and Savel'yev [Reference 2-17]. Figure 2-7 sketches the geometry of their experiment. Figure 2-8, reproduced from their paper, shows fast amplitude scintillations developing 2 minutes after the OTH was turned on. Phase fluctuations between receivers spaced by several hundred meters increased in amplitude and became more rapid. Further measurements determined that the scale size of ionospheric striations was $\approx$ 300 m and that the spread of arrival angles at the diagnostic receiver increased from $\pm$ 0.3° to $\pm$1°. According to Novozhilov and Savel'yev, the

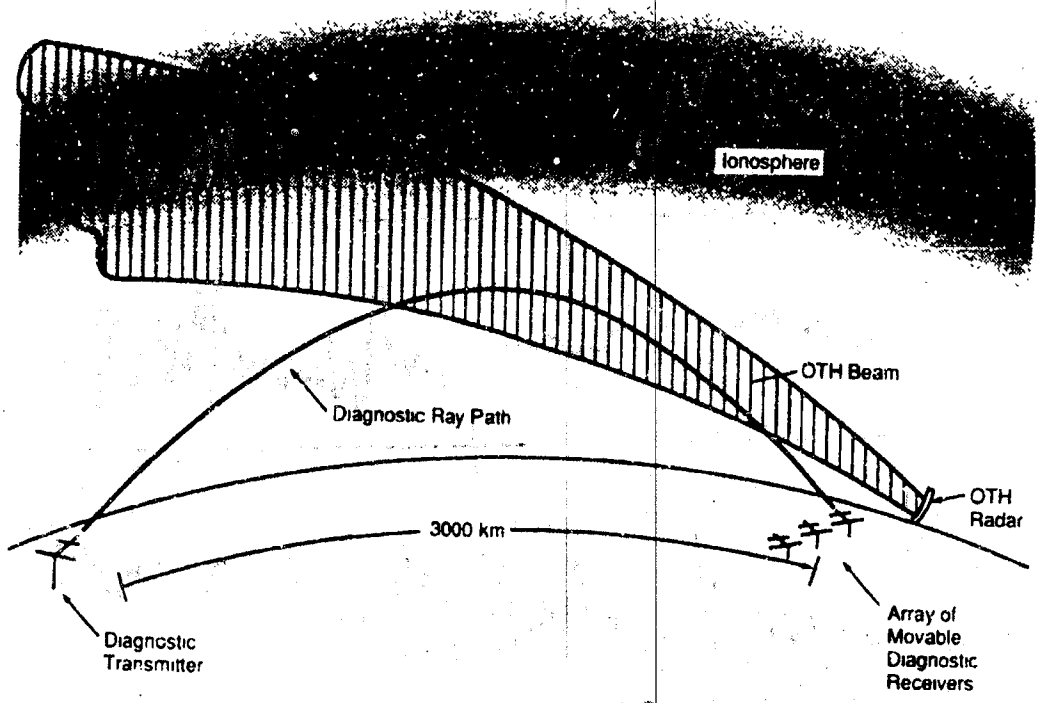

Figure 2-7. Geometry of the Novozhilov and Savel'yev experiment, performed near 1500 h, April 17, 1975. The OTH frequency ν was not reported; it slightly exceeds the maximum usable frequency (MUF). We assume $\nu \approx 30$ MHz appropriate to daytime conditions; the diagnostic frequency was then about 25 MHz.

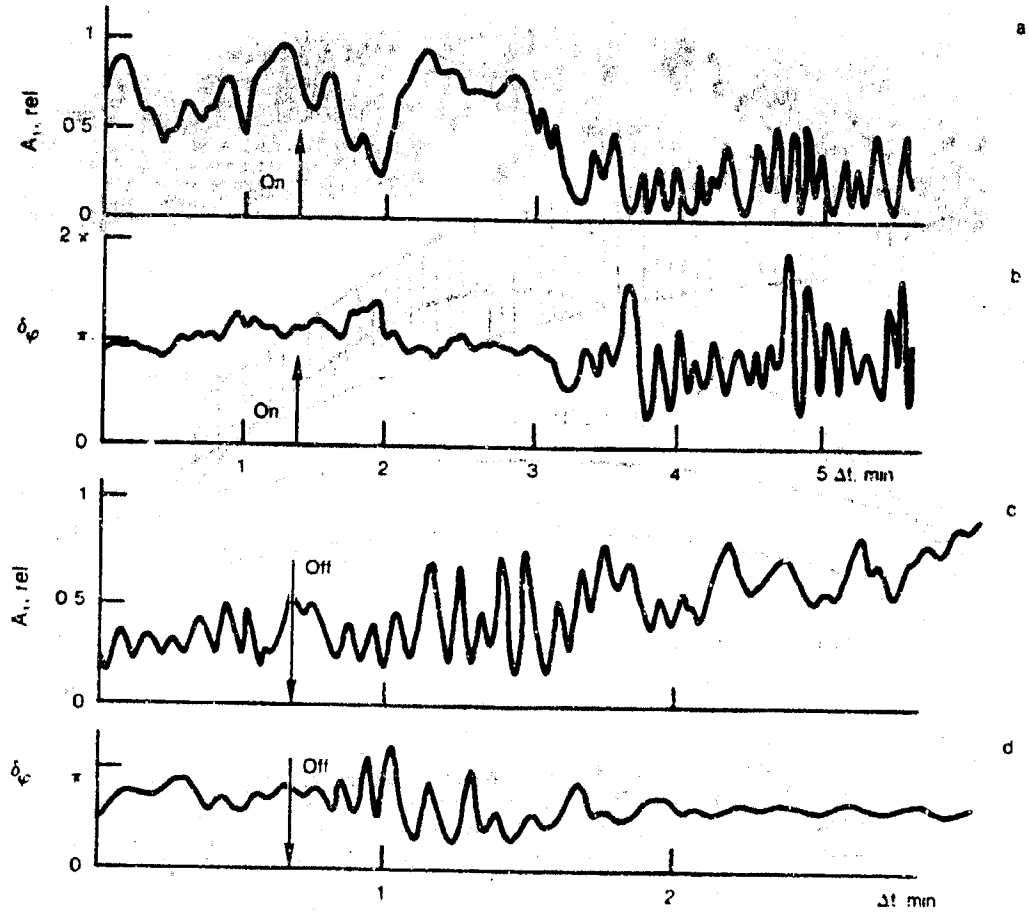

Figure 2-8. Results for Novozhilov and Savel'yev experiment a) Amplitude scintillation commences ≈ 2 min after OTH turn-on, b) Phase fluctuations between two receivers spaced by several hundred meters commence ≈ 2 min after OTH turn-on, c) and d) Amplitude and phase fluctuations decay ≈ 1 min after OTH turn-off Source Reference 2-16

HF electric field in the ionosphere was $E_o \approx (0.1)E_p$ where E_p, is the plasma field defined by Gurevich [Reference 2-18] as

$$E_p^2 = \frac{3T_e m_e}{e^2}\delta\omega^2, \qquad \delta = \frac{2m_e}{M_i}. \tag{2-5}$$

Here δ denotes the average energy lost by an electron in an electron-ion collision. We shall argue below that self-focusing instabilities are most virulent when the electron collision frequency is high, which is obtained when plasma density is high, electron temperature low, and electron-ion collisions dominate electron-neutral collisions. For an O^+ plasma, one has $\delta = 7 \cdot 10^{-5}$ and the power flux through the ionospheric plasma is

$$F_o \approx (0.1)^2 \frac{c}{4\pi} E_p^2 \approx 10^{-4}\ \mathrm{W/m^2}, \tag{2-6}$$

where we have assumed $T_e \approx 1,000°\mathrm{K}$ and a frequency $\nu \approx 30$ MHz for daytime OTH operation.

2.3.1 OTH Ray Trajectories and Ionospheric Power Flux

Let us employ ray-tracing to estimate the power flux of an OTH radar based on a simple parabolic model of the electron density below the peak of the F-region. The plasma frequency profile is

$$\omega_p^2 = \omega_{p,max}^2[1 - (\frac{z}{z_o})^2], \tag{2-7}$$

where $\omega_{p,max}$ denotes the maximum plasma frequency and $z_o \approx 100$ km. From the simplified-but-adequate dispersion relation

$$\begin{aligned} \omega^2 &= \omega_p^2 + (k_h^2 + k_z^2)c^2 \\ &= \omega_p^2 + \omega^2\cos^2\theta + c^2k_z^2, \end{aligned} \tag{2-8}$$

we can compute horizontal and vertical group velocities

$$V_h = c\ \cos\theta \quad V_z = c\left[\sin^2\theta - \frac{\omega_{p,max}^2}{\omega^2}\left(1 - \frac{z^2}{z_o^2}\right)\right]^{1/2}. \qquad (2-9)$$

Here θ denotes the initial elevation angle of the ray. From the ray equation in the ionosphere

$$dR = \frac{V_h dz}{V_z} = \frac{\omega\cos\theta dz}{\omega_{p,max}\left[\frac{z^2}{z_o^2} - 1 + \frac{\omega^2\sin^2\theta}{\omega_{p,max}^2}\right]^{1/2}}, \qquad (2-10)$$

we can compute the relation between range R, ionospheric height z, and initial launch angle θ. For a ray that is still ascending, we can integrate (2-10) to obtain

$$R^+ = \frac{H}{\tan\theta} + \frac{z_o\cos\theta\,\omega}{\omega_{p,max}}\,ln\left\{\frac{1 + \frac{\omega\sin\theta}{\omega_{p,max}}}{\frac{z}{z_o} + \left[(\frac{z}{z_o})^2 - 1 + \frac{\omega^2\sin^2\theta}{\omega_{p,max}^2}\right]^{1/2}}\right\} \qquad (2-11)$$

in a flat-earth approximation, which is adequate for our estimate of the power flux.

At a fixed range, Equation (2-11) relates the ray height in the ionosphere to launch elevation angle θ. It is straightforward to generalize Equation (2-11) for descending rays that have reflected from the height where

$$(\frac{z}{z_o})^2 = 1 - \frac{\omega^2\sin^2\theta}{\omega_{p,max}^2}. \qquad (2-12)$$

The range formula for descending rays is

$$R^- = \frac{H}{\tan\theta} + \frac{z_o\cos\theta\omega}{\omega_{p,max}}\,ln\left\{\frac{(1 + \frac{\omega\sin\theta}{\omega_{p,max}})[\frac{z}{z_o} + (\frac{z^2}{z_o^2} - 1 + \frac{\omega^2\sin^2\theta}{\omega_{p,max}^2})^{1/2}]}{1 - \frac{\omega^2\sin^2\theta}{\omega_{p,max}^2}}\right\}. \qquad (2-13)$$

When we set $z/z_o = 1$, we can determine the total horizontal distance ΔR_{ion} travelled by the ray in the ionosphere

$$\Delta R_{ion} = \frac{z_o\cos\theta\omega}{\omega_{p,max}}ln\left\{\frac{(1 + \frac{\omega\sin\theta}{\omega_{p,max}})^2}{1 - \frac{\omega^2\sin\theta}{\omega_{p^2,max}}}\right\} \qquad (2-14)$$

$$\simeq \frac{2z_o}{\tan\theta}\left(\frac{\omega\sin\theta}{\omega_{p,max}}\right)^2 \quad , \quad \frac{\omega\sin\theta}{\omega_{p,max}} << 1. \qquad (2\text{-}15)$$

For most long-range OTH operations, which utilize low rays, the form (2-15) is valid. The range R at which the ray strikes the earth is

$$R(\theta) = \frac{2H}{\tan\theta} + \Delta R_{ion}. \qquad (2-16)$$

Using the characteristic values $H \approx 200$ km, $z_o \approx 100$ km, we find that the contribution of ΔR_{ion} to (2-16) is small when $(\omega\sin\theta/\omega_{p,max}) \ll 1$. Thus to a good approximation

$$\tan\theta \approx \frac{2H}{R}. \qquad (2-17)$$

Let us note that because the denominator of the logarithm in Equation (2-14) diverges as $\sin\theta \rightarrow \omega_{p,max}/\omega$, there are two θ values corresponding to a given range, the low ray which has $(\omega\sin\theta/\omega_{p,max}) \ll 1$ and a high ray with $\sin\theta \approx \omega_{p,max}/\omega$, independent of range. Since all high rays correspond to a very small interval in elevation angle θ, the power launched onto high rays is negligible. Thus, we need to consider only low rays in estimates of ionospheric power density; Equations (2-15) and (2-17) are good approximations.

The power density in the ionosphere at a range R_{ion} follows from the formula

$$F_o = \frac{1}{R_{ion}}\left(\frac{\partial^2 P}{\partial\phi\partial\theta}\right)\left[\left|\frac{d\theta^+}{dz}\right| + \left|\frac{d\theta^-}{dz}\right|\right]_{\tan\theta = H/R_{ion}}, \qquad (2-18)$$

where $(\partial^2 P/\partial\phi\partial\theta)$ is the transmitter beam pattern in azimuthal angle ϕ and elevation angle θ and

$$\frac{d\theta^+}{dz} = \frac{\left(\frac{\partial R^+}{\partial z}\right)_\theta}{\left(\frac{\partial R^+}{\partial\theta}\right)_z} \qquad (2-19)$$

with an evident generalization for the contribution from descending rays. Following our approximation for low rays, we find

$$|\frac{d\theta^+}{dz}| + |\frac{d\theta^-}{dz}| \approx \frac{2\sin\theta\cos\theta}{H}\left(\frac{\omega\sin\theta}{\omega_{p,max}}\right)\frac{1}{[\frac{z^2}{z_o^2} - 1 + \frac{\omega^2\sin^2\theta}{\omega^2_{p,max}}]^{1/2}} \qquad (2-20)$$

$$\approx \frac{2}{R_{\rm ion}}\left(\frac{\omega\sin\theta}{\omega_{p,max}}\right)\frac{1}{[\frac{z^2}{z_o^2} - 1 + \frac{\omega^2\sin^2\theta}{\omega^2_{p,max}}]^{1/2}}. \qquad (2-21)$$

Within the context of ray optics, the power flux diverges at the reflection height. Since we shall show that self-focusing instabilities are extended along magnetic field lines for distances $\sim$ 5 km, it is meaningful to compute the average power flux in the ionosphere. We define this as

$$< F_o >= \frac{1}{z_o - z_1}\int_{z_1}^{z_o} dz\, F_o(z), \qquad (2-22)$$

where $z_1 = z_o(1 - \frac{\omega^2\sin^2\theta}{\omega^2_{p,max}})^{1/2}$ is the reflection height. Again using low-ray approximations, we find that

$$< F_o >= \frac{4}{R^2_{\rm ion}}\frac{\partial^2 P}{\partial\phi\partial\theta}, \approx \frac{4}{R^2_{\rm ion}}\frac{P_T}{\Delta\Omega} = \frac{1}{\pi R^2_{\rm ion}}(P_T G) \qquad (2-23)$$

where $P_T G$ is the effective radiated power (ERP) and $\Delta\Omega$ estimates the solid angle of the transmitter beam. We can combine Equations (2-18), (2-21), and (2-23) to obtain an expression for the altitude-dependent power density,

$$F_o(z) = \frac{1}{2} < F_o > \frac{1}{[1 - (\frac{z_o - z}{\Delta z})]^{1/2}} = \frac{P_T G}{2\pi R^2_{\rm ion}}\frac{1}{[(1 - (\frac{z_o - z}{\Delta z})]^{1/2}}, \qquad (2-24)$$

where

$$\Delta z \approx z_o\omega^2\sin^2\theta/2\omega^2_{p,max} \qquad (2-25)$$

in a low-ray approximation. Suppose a nominal OTH antenna radiates into an azithumal sector $\Delta\phi \approx 10°$ and has an $\Delta\theta \approx 45°$ beam width in elevation angle. We then find

$$< F_o >= (30\frac{\mu W}{\rm m^2})\,(\frac{P}{1\rm MW})\,(\frac{10^6\rm m}{R_{\rm ion}})^2. \qquad (2-26)$$

From this we deduce that the Soviet transmitter power was $P \approx 10$ MW to agree with (2-6). The gain of our nominal OTH transmitter is $G = 4\pi/\Delta\Omega \approx 100$. Hence the ERP of the Soviet OTH installation is estimated to be 90 dBw. MITRE's proposed ETB transmitting antenna has an ERP of 95 dBw giving it a power flux of $3 \cdot 10^{-4}$ W/m^2 at a range of 1,500 km. Our theoretical development below places the threshold flux for self-focusing at about 10^{-4} W/m^2 during daytime conditions. (It will be significantly higher at night.)

We conclude this section by noting that OTH-induced self-focusing instabilities have been observed by Soviet researchers and that the power fluxes estimated from their paper agree with those produced by a nominal 10 MW OTH radar with an ERP of 90 dBw. An ETB is proposed to have an ERP of $\approx$ 95 dBw and a full-capability AOTH system $\approx$ 97 dBw per transmit beam. Thus, experimentally, we should expect that self-focusing striations could arise in ETB and AOTH systems.

2.3.2 Self-Focusing Instability Analysis

A detailed theoretical analysis of the self-focusing instability has been published by Perkins and Goldman [Reference 2-16]. We shall abstract the essential physics from this paper. It suffices to consider a strong electromagnetic wave propagating in a underdense, uniform plasma $\omega > \omega_p$. The geometry of self-focusing striations is field-aligned sheets of density irregularities with a wave vector q which lies in the direction $\vec{k_o} \times \vec{B}$, where $\vec{k_o}$ denotes the wave vector of the strong electromagnetic wave and $\vec{B}$ the earth's magnetic field. The density irregularities grow exponentially both spatially along

the direction of $\vec{k_o}$ and temporally. Figure 2-9 gives the coordinate system for our computation. We assume that density perturbations δn and other dependent variables take the form

$$\delta n = \tilde{n}(\xi) e^{iqy + \alpha(x + z\tan\beta) + \gamma t},$$

where

$$\begin{aligned} \eta &= x\cos\beta + z\sin\beta \\ \xi &= x\sin\beta - z\cos\beta \end{aligned}$$

and β denotes the angle of the geomagnetic field with respect to vertical. We make the assumption, readily justified a posteriori, that $q \gg \frac{\partial}{\partial z}, \frac{\partial}{\partial x}$ when acting on δn.

The equations governing self-focusing instabilities are

$$\begin{aligned} \tilde{F} &= - F_o(\xi) \frac{\omega_p^2 \Delta}{\omega_o c} \int_{-\infty}^{x} \sin[\frac{q^2(x-x')}{2k_o}] e^{-\alpha(x-x')}\, dx' \qquad (2\text{-}27) \\ &= - F_o(\xi) \frac{\omega_p^2 \Delta}{2\omega_o c\alpha} (\frac{2\epsilon}{1+\epsilon^2}) \end{aligned}$$

$$\gamma\Delta = 2D\frac{\partial^2 \Delta}{\partial \xi^2} + D\frac{\partial^2 \tau}{\partial \xi^2} \qquad (2-28)$$

$$K\frac{\partial^2}{\partial \xi^2}\tau + \frac{\omega_p^2 \nu_e}{T\omega_o^2 c}\tilde{F} = 0. \qquad (2-29)$$

Here we use the definition $\tau = \tilde{T}/T, \Delta = \tilde{n}/n$, and

$$\epsilon = \frac{q^2}{2k_o\alpha}, \qquad K = 3.16Tn/m\nu_e, \qquad D = T/M\nu_{in}. \qquad (2-30)$$

To a good approximation $\omega_o = k_o c$, since $\omega_o^2 \gg \omega_p^2$.

Let us briefly describe the physics content of each equation. Equation (2-27) gives the intensity fluctuations at x resulting from phase perturbations

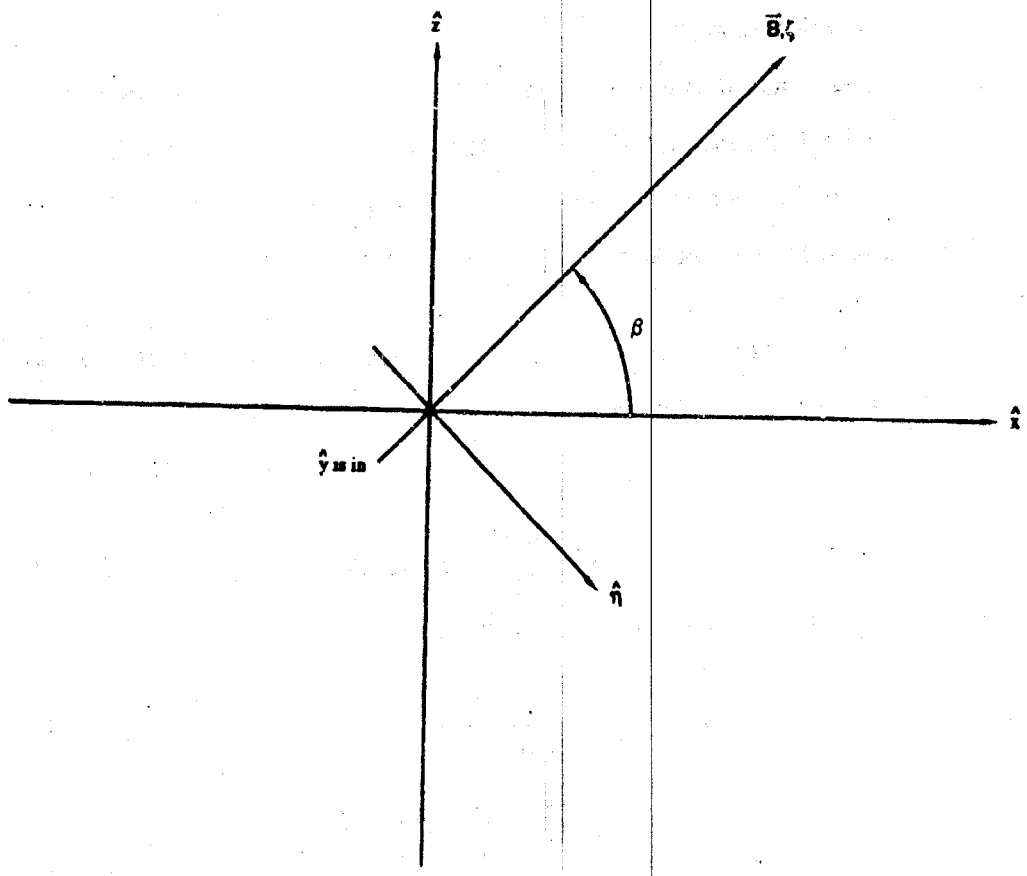

Figure 2-9. Coordinate system for self-focusing instability calculations. The intense wave propagates in the $\hat{x}$ direction.

caused by index of refraction fluctuations at x'. Equation (2-4) links the index of refraction to density. Equation (2-29) governs electron temperature fluctuations resulting from differential heating due to intensity fluctuations. The dominant limitation on temperature fluctuations comes from electron heat conduction along magnetic field lines to a constant temperature bath. This makes sense if the strong beam $F_o(\xi)$ is spatially limited along the magnetic field. Equation (2-28) states that plasma density fluctuations arise because ions diffuse through neutrals along the geometric field, the diffusion being driven by electron temperature fluctuations.

Straightforward algebra enables us to combine Equations (2-27) through (2-29) into the eigenvalue equation

$$\Delta - \frac{2D}{\alpha}\frac{\partial^2\Delta}{\partial\xi^2} = \Lambda\Theta(\xi)\Delta, \qquad (2-31)$$

where from Equations (2-18) through (2-21)

$$\Lambda = \frac{\omega_p^2\nu_e^2\pi\epsilon^2 < F_o >}{M\nu_{in}\gamma\omega_o^3(3.16)T\alpha C^2}\left(\frac{2\epsilon}{\epsilon^2+1}\right) \qquad (2-32)$$

$$0 = \begin{cases} \left(\frac{\xi}{\xi_o}\right)^3 \frac{1}{(1-\frac{\xi}{\xi_o})^{1/2}} & \xi < \xi_o \\ 0 & \xi > \xi_o \end{cases} \qquad (2-33)$$

$$\xi_o = \frac{z_o}{2}\frac{\omega_o^2\sin^2\theta}{\omega_{p,max}^2\cos\beta} = \frac{\Delta z}{\cos\beta} \approx 20\text{ km}\left(\frac{1000\text{ km}}{R_{ion}}\right)^2 \qquad (2-34)$$

and the electron density is to be evaluated at a point where $\omega_p^2 = \omega_o^2\sin^2\theta$.

Let us rescale the z-variable according to

$$\begin{aligned} \xi_o - \xi &= U_o u \qquad (2\text{-}35) \\ U_o = \left(\frac{2D}{\gamma}\right)^{1/2} &= 3\text{km}\left(\frac{T}{10^3 K}\right)^{1/2}\left(\frac{10^{-1}\text{sec}}{\gamma}\right)^{1/2}\left(\frac{1\text{Hz}}{\nu_{in}}\right)^{1/2}. \end{aligned}$$

Note that ξ_o is appreciably longer than U_o, so Equation (2-31) can be adequately approximated by

$$\frac{\partial^2 \Delta}{\partial u^2} - \Delta = -\frac{\lambda \Delta}{u^{1/2}}, \qquad (2-36)$$

where $0 < u < \infty$, and

$$\lambda = \Lambda(\xi_o/U_o)^{1/2}. \qquad (2-37)$$

is an eigenvalue of order unity. The boundary conditions for (2-36) are

$$\frac{1}{\Delta}\frac{\partial \Delta}{\partial u} = 1, \qquad u = 0 \qquad (2\text{-}38)$$

$$\frac{1}{\Delta}\frac{\partial \Delta}{\partial u} = -1, \qquad u \to \infty. \qquad (2\text{-}39)$$

Thus the critical flux for self-focusing instabilities is

$$< F_o >= F_c \equiv \left(\frac{3.16\lambda}{\pi}\right) \frac{M\, \nu_{in} \gamma\, \omega_o^3\, T\, \alpha c^2}{\omega_{pe}^2 \nu_e^2 e^2} \left(\frac{U_o}{\xi_o}\right)^{1/2} \left(\frac{\epsilon^2+1}{2\epsilon}\right). \qquad (2-40)$$

We can cast (2-40) into practical units and obtain

$$F_c = (0.3\,\frac{\mu W}{m^2}) \left(\frac{n_{max}}{n}\right)^2 \left(\frac{10^5 \mathrm{cm}^{-3}}{n_{max}}\right)^{3/2} \left(\frac{25\mathrm{km}}{\alpha^{-1}}\right) \left(\frac{100\mathrm{km}}{z_o}\right)^{1/2}$$

$$\left(\frac{T}{10^2 K}\right)^{4.25} \left(\frac{\gamma}{10^{-1}\mathrm{s}}\right)^{3/4} \left(\frac{\nu_{in}}{1\mathrm{Hz}}\right)^{3/4} \frac{(\cos\beta)^{1/2}}{\sin^2\theta} \left(\frac{\epsilon^2+1}{2\epsilon}\right), \qquad (2-41)$$

where we have used $\omega_o \sin\theta = \omega_p$. For representative OTH operations, we has

$$\sin\theta \approx 0.2 \qquad (2\text{-}42)$$

$$n/n_{max} \approx 0.5.$$

Assuming all other factors are unity, we obtain

$$F_c \approx 1.5 \cdot 10^{-4} \frac{W}{m^2} \qquad (2-43)$$

in good accord with observations. Further note that the critical flux is minimum for $\epsilon = 1$, corresponding to $\lambda_{perp} = 2\pi/q \approx 1.2$ km$(\alpha^{-1}/25$ km$)^{1/2}$. Again, there is agreement with Novozhilov and Savel'yev.

In evaluating (2-41), we assumed an exponentiation time of 10 s to obtain a modestly large number of e-foldings in one minute. Similarly, the spatial growth length of 25 km is moderately small compared to the distance a ray spends in the ionosphere.

When will self-focusing instabilities affect OTH operations? OTH radars continuously transmit power into an angular sector with FM modulation which provides range resolution upon processing. The FM nature of the transmit signal plays no role in self-focusing instabilities. We see from Equation (2-23) that an ERP at 87 dBw is required to exceed the threshold value of (2-41) during high-density low-T_e daytime conditions. Noting that, for OTH operations, $f^2 \propto n_{max}$ it follows from (2-40) that $F_c \propto f^{-3}$. In other words, the instability becomes appreciably less important at night. It is also stabilized by high electron temperatures, often, but not always, a feature of daytime ionospheres. High temperatures reduce the electron-ion collision frequency, which diminishes resistive heating, and increase electron thermal conductivity, both stabilizing effects. Lastly, we note that growth times are near 10 s, comparable to the planned OTH coherent integration times. We can certainly tolerate one e-folding of fluctuations, so rapid beam switching will defeat self-focusing instablilities near threshold. The eventual AOTH system plans an ERP of 97 dBw in each of 12 beams which exceeds the threshold flux by a factor of 10, reducing the growth time to $\sim$ 1 s under daytime conditions.

The planned ERP of 95 dBw for ETB should be well into the regime where self-focusing arises in daytime conditions. ETB should be able to investigate self-focusing instabilities. From a practical point-of-view, we may not need the full ERP of AOTH in daytime conditions. As the frequency falls from 30 MHz to 6 MHz, the threshold ERP increases from 87 dBw to

120 dBw. Since AOTH is planned to operate with 97 dBw per beam, it is predicted to be free of self-focusing instabilities when target cross sections are low at nighttime.

2.4 Radio Noise at HF

2.4.1 Atmospheric Noise Characteristics

Radio noise resulting from lightning discharges is the dominant atmospheric noise within the HF band where OTH radars operate. Generally the level of atmospheric noise increases as the operating frequency decreases, and has strong diurnal variation. Increased levels of thunderstorm activity in the late afternoon, coupled with absorption decreases in the ionospheric D-region, result in significant increases in the observed noise level during these times. The OTH radar-detection problem is aggravated by the fact that operating frequencies are generally lower at night than during the daytime, which results in a decrease in the radar cross section of small targets and a consequent degradation in system performance. Understanding the characteristics of external noise is an important aspect of the residual clutter and noise issue for AOTH radars.

Extensive investigations have been conducted over the past 30 years to characterize this noise. However, the analysis has focused on communication system applications. In general, atmospheric noise is impulsive with the high amplitude, low probability of occurrence values controlling the noise ampli-

tude distribution and the expected RMS value of the noise F_a. The impulsive short-term characteristics of the noise are estimated from a parameter called V_d, which indicates a deviation between the average voltage and the RMS value of the noise. The parameters F_{am} (the median value of F_a) and V_{dm} (the median value of V_d) are presented in CCIR Report 322 [Reference 2-19] as functions of geographic position, season, local time of day, and frequency.

The CCIR 322 atmospheric noise collection procedures were developed through international cooperation. Recording stations at various locations were instrumented to record selected statistical parameters of atmospheric noise at specific frequencies. Man made noise, interference, and atmospheric noise from local thunderstorms were excluded from the analysis. The noise measuring equipment was the ARN-2, which uses a 200-Hz analysis bandwidth. The recording process involved the use of a calibrated short vertical whip antenna with stepped attenuators controlled by the averaged RMS value of the noise. A four-minute integration time was used to calculate the RMS value of the noise. If the RMS value changed by more than 2 dB during the four-minute measurement period, the data were excluded from the data base, since changes larger than this were interpreted to result from man-made noise, interference, or local thunderstorms. The recorded RMS level, attenuation value, and antenna calibration parameters were then used to calculate the external noise level. The difference between the RMS voltage and the average voltage V_d, and the difference between the RMS and the average of the logarithm of the voltage L_d were also recorded. These data were then analyzed by frequency, season, and four-hour time periods. The median RMS noise value F_{am} and median value of voltage deviation V_{dm} are presented in CCIR 322, together with the corresponding upper and lower decile values and the standard deviations of the measurements. The use of four-minute

integration period for estimating the RMS value of the noise implies a minimum period to achieve stationarity. Figure 2-10 shows noise characteristics as presented in CCIR 322. Note the concentration of noise in the Caribbean region and in South East Asia.

2.4.2 Lightning-Produced HF Noise

Horner [Reference 2-20] made a comprehensive study of close-by atmospherics at different frequencies. In particular he showed that, in disagreement with current theory, HF waveforms could not be accounted for strictly by return strokes and stepped leader processes. He suggested that the in-cloud processes occurring during the intervals between return strokes were the cause of most HF radiation.

Using receiver bandwidths of over 100 kHz, Oetzel and Pierce [Reference 2-21] found that HF atmospherics were comprised of several hundred to over a thousand impulses. The bandwidth of typical HF communications receivers is too narrow to resolve this impulse train. Thus at the output of such a receiver, an HF atmospheric usually takes the form of a nearly continuous burst of noise. On the other hand, AOTH bandwidths are proposed to be much larger, as high as 1 MHz.

Horner pointed out that the structure of HF atmospheric noise would become more variable when received on a directional antenna. Horner also made an attempt to infer specific information from individual HF atmospherics propagated via skywave. Receiving the same atmospheric at different HF frequencies, he was able to use predictions of propagation conditions to esti-

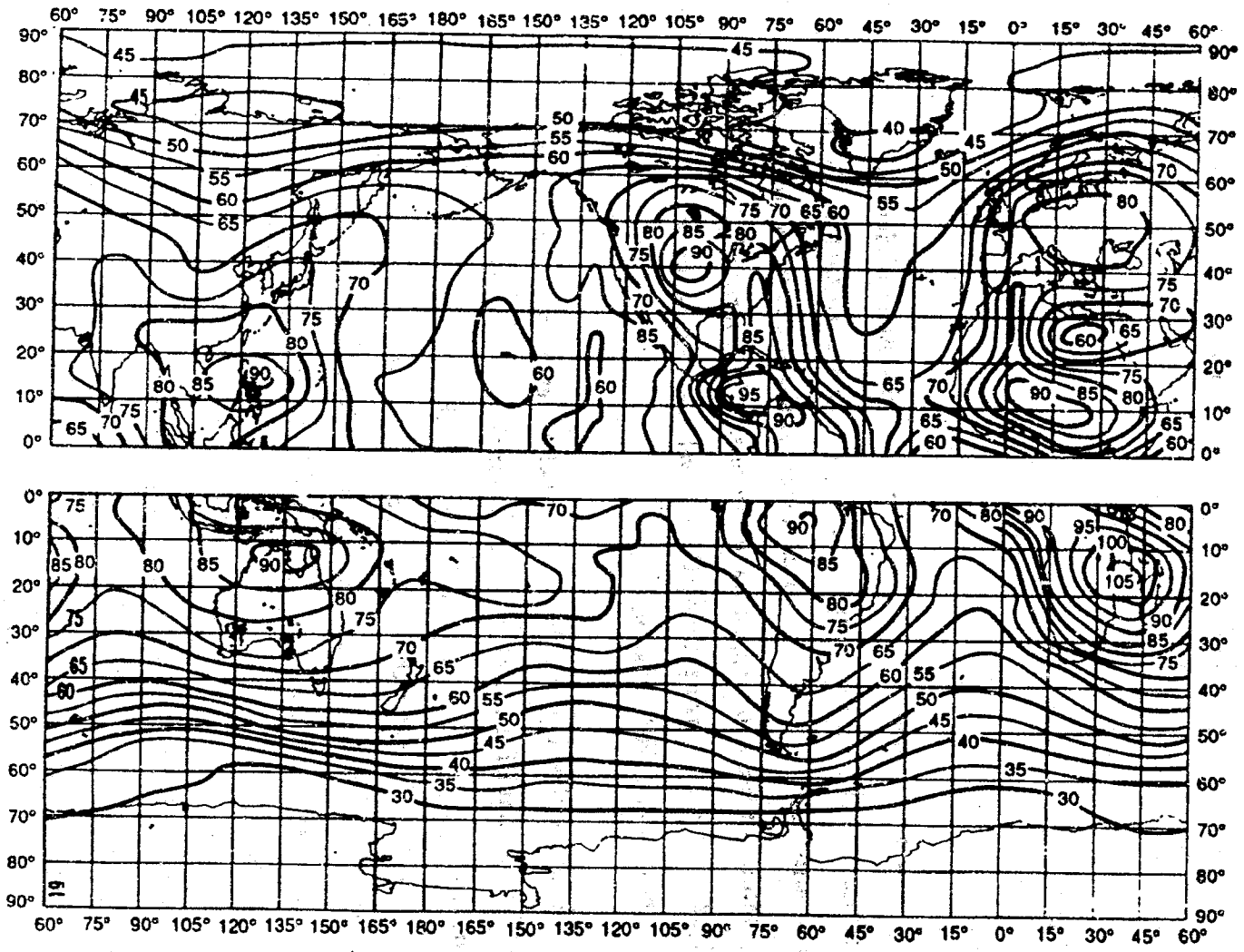

Figure 2-10a. Expected values of atmospheric radio noise F_{am} (dB above kT_0b at 1 MHz) (Summer; 2000-2400 h.)
Source Reference 2-19

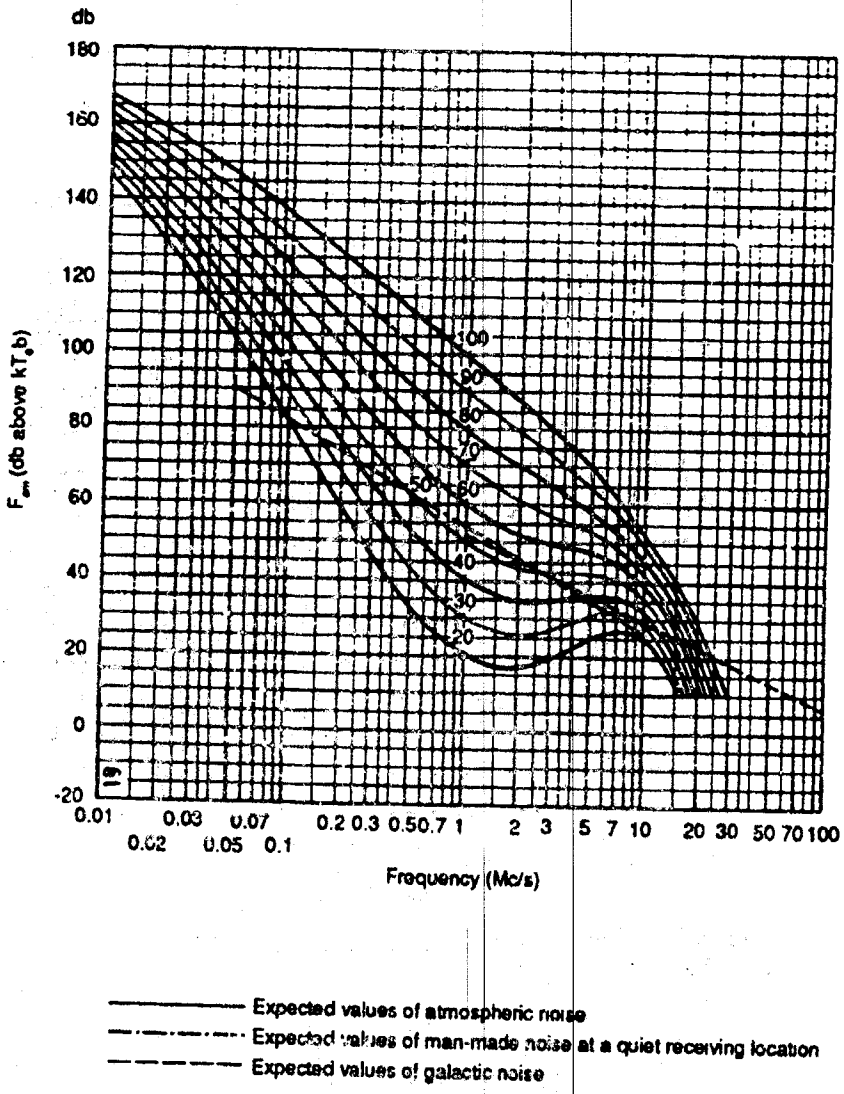

Figure 2-10b. Variation of radio with frequency (Summer, 2000-2400 h)
Source: Reference 2-19.

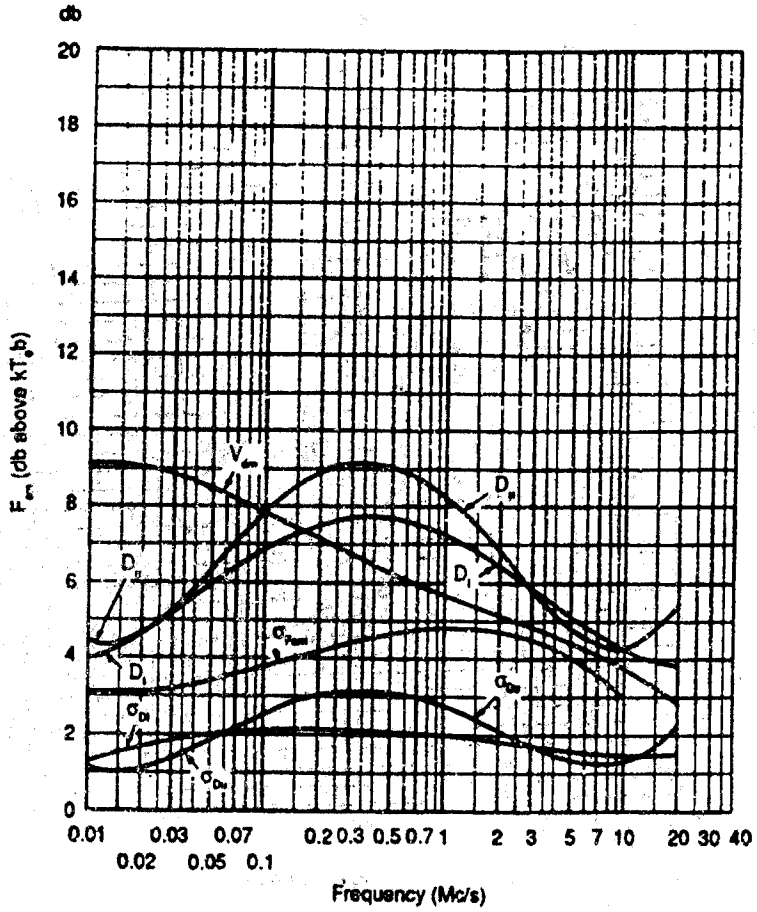

Figure 2-10c. Data on noise variability and character (Summer; 2000-2400 h.) Source: Reference 2-19.

σ_{Fam} = Standard deviation of values of F_{am}.

D_u = Ratio of upper decile to median value, F_{am}.

σ_{Du} = Standard deviation of values of D_u.

D_l = Ratio of median value, F_{am} to lower decile.

σ_{Dl} = Standard deviation of value of D_l.

V_{dm} = Expected value of median deviation of average voltage. The values shown are for a bandwidth of 200 c/s.

mate the range of the flash to an accuracy of 100 km.

With the appropriate meteorological conditions, thunderstorms can develop giant proportions. These thunderstorms are classified as severe if they produce at least one of the following: a tornado, funnel cloud, waterspout, hail (greater than 0.75 inch diameter), wind gusts (greater than 50 knots), or extreme upper-air turbulence. The intensely active electrical nature of severe storms has often been noted and unusual lightning has even been observed within the actual tornado vortex. In 1950, Jones reported that VLF atmospherics radiated from severe thunderstorms exhibit identifiable characteristics, thus suggesting a potential mechanism for severe thunderstorm warnings.

2.4.3 Experimental Observations of Noise Characteristics Versus Antenna Directivity

To test the effect of antenna directivity on the characteristics of received HF noise, data were recorded using the 0.5° WARF antenna and an omnidirectional vertical monopole situated about 100 m away [Reference 2-22]. HF noise was simultaneously received on two matched receivers of 1.4 kHz bandwidth. The data were recorded on a summer afternoon when no local storm activity was present. The WARF antenna was pointed in the general direction of known midwestern thunderstorm activity.

Each receiver output was sampled at a 500-Hz rate. The RMS value, E_{rms}, computed over five samples (corresponding to 1 ms) was used to estimate the noise envelope. These 1-ms samples were calculated for a 30-s

interval of data and used to construct empirical amplitude-probability distributions. Representative samples of the resulting distributions are shown in Figure 2-11. These cumulative distributions have been plotted on Rayleigh probability paper, which has the characteristic that a Rayleigh distribution takes the form of a straight line of slope -0.5. The distributions of Figure 2-11 exhibit low-amplitude Rayleigh components.

The distributions in Figure 2-11a have been normalized by the RMS average of their envelopes in accordance with the conventions used by the authors mentioned above. However, for the purpose of comparing the distributions obtained from different antennas, it is convenient to equalize the common Rayleigh noise "background." This was accomplished in Figure 2-11b by renormalizing the distributions by their respective mode[1] values.

From Figure 2-11b, it is evident that the high-amplitude component of the observed atmospheric noise is more pronounced for the directional antenna. Review of the data in the time domain is necessary to determine if this component is produced by individual atmospherics. Figure 2-12 plots one-second intervals of the data used to compute the distributions of Figure 2-11. The envelope of the noise received with the two different antennas has been normalized by their respective mode values to provide equal noise backgrounds. It can be seen that most of the high-amplitude values are clustered in discrete bursts. Although hardly observable on the monopole data, the time/amplitude characteristics of the noise bursts received on the directional antenna are similar to observations of single HF atmospherics radiated from close lightning flashes. (The receiver passband was too narrow to resolve individual impulses and the atmospheric therefore takes the form

[1]The mode represents the value for which the amplitude-probability density function attains its maximum.

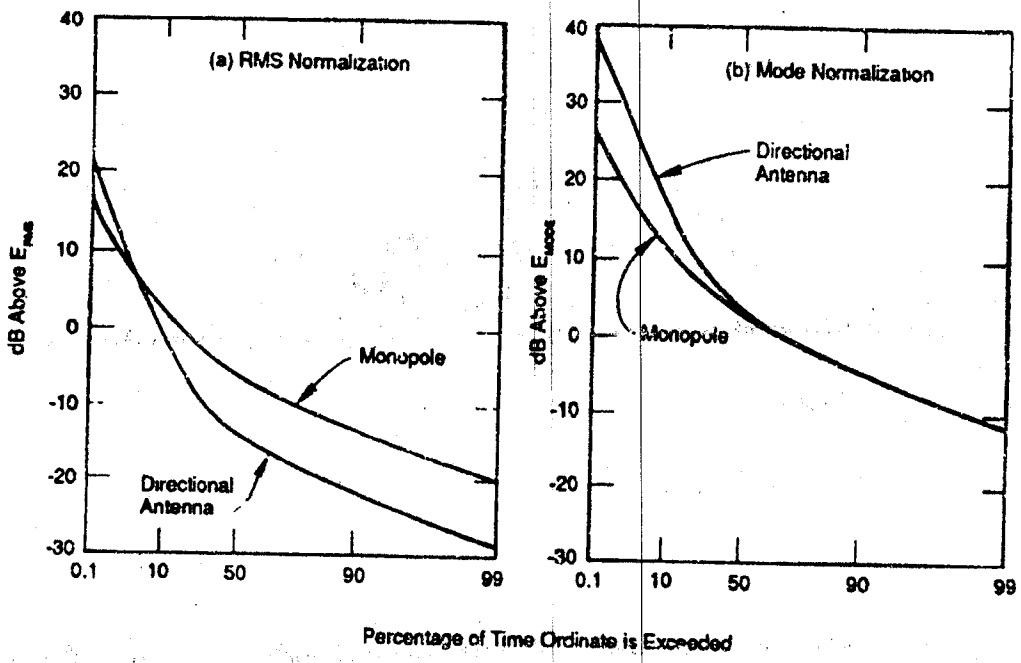

Figure 2-11. Cumulative amplitude-probability distributions of noise received on antennas of different directivity. Source: Reference 2-22.

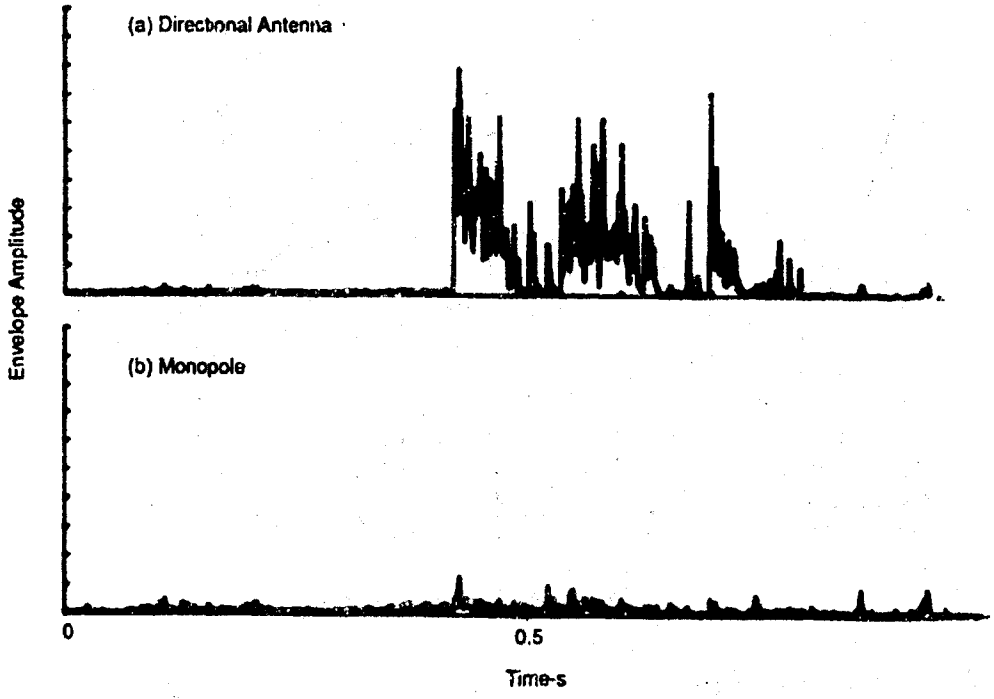

Figure 2-12. Envelope of receiver output vs. time. Source: Reference 2-22.

of a continuous burst of noise.) Furutsu showed that HF noise distributions with such unusually strong amplitude components can be caused when local thunderstorms are present. But, since no local storms were present, the weight of evidence suggests that these strong atmospherics originated from remote flashes (presumably at a one-hop distance) and were received via skywave propagation.

2.4.4 Verification of the Source of Atmospherics Observed with the Directional Antenna

The observations described in the previous section imply that many of the strong and well-defined atmospherics received on the WARF antenna originate at a remote distance and then propagate to the antenna via skywave. Direct verification of this hypothesis was made by field measurements [Reference 2-22]. An experiment was designed to record and compare signals received on the 0.5° antenna with measurements at a one-hop distance from northern California.

A remote field site was established in an area of New Mexico likely to produce thunderstorm activity. When a storm approached this site, HF noise data were simultaneously recorded there and in California with the 0.5° antenna pointed in the storm's direction. Wide-sweep backscatter soundings were taken at WARF to determine the best band of frequencies available for propagation to the remote side and thereby infer, by reciprocity, the best frequency band available from the remote site to WARF. The 1.4 kHz receivers of both sites were then tuned to an interference-free channel within this frequency band. This selection process was principally accomplished

by listening to the receiver output for the presence of man-made signals. Simultaneous HF records were then collected at both sites for use in making a comparison of atmospheric noise received via direct and one-hop paths.

ELF records were also recorded at the field site. These records were intended for use in identifying flashes close to the site. The characteristics of ELF radiation from lightning change rapidly with propagation distance. At close ranges the electrostatic field is strong, but this field decreases in proportion to the cube of distance. The weaker radiation field, which decreases linearly with distance, will predominate at longer ranges. The reception of ELF radiation indicative of a strong electrostatic component can thus be used to identify flashes occurring close to the field site. The simple form of the electrostatic field can also be used to identify specific events within a lightning flash. Figures 2-13a and 2-13c show ELF measurements recorded in New Mexico while Figures 2-13b and 2-13d show the HF noise at WARF in California.

2.4.5 Noise Observed on Whip Antenna at WARF in 1986

Analysis of transmitter-off noise data collected at WARF [Reference 2-23] indicates that the noise is impulsive, as expected, and that for CITs (coherent integration times) in excess of about 1 to 2 seconds (analysis bandwidth less than 1 Hz), the noise amplitude is Rayleigh distributed across the range-doppler transform. The presence or absence of impulsive events is observed to change the dwell-to-dwell noise level by 3 dB to 10 dB depending on the operating frequency and CIT. Measurement of the median or average RMS level spanning a minute or more yields a stable estimate of the noise

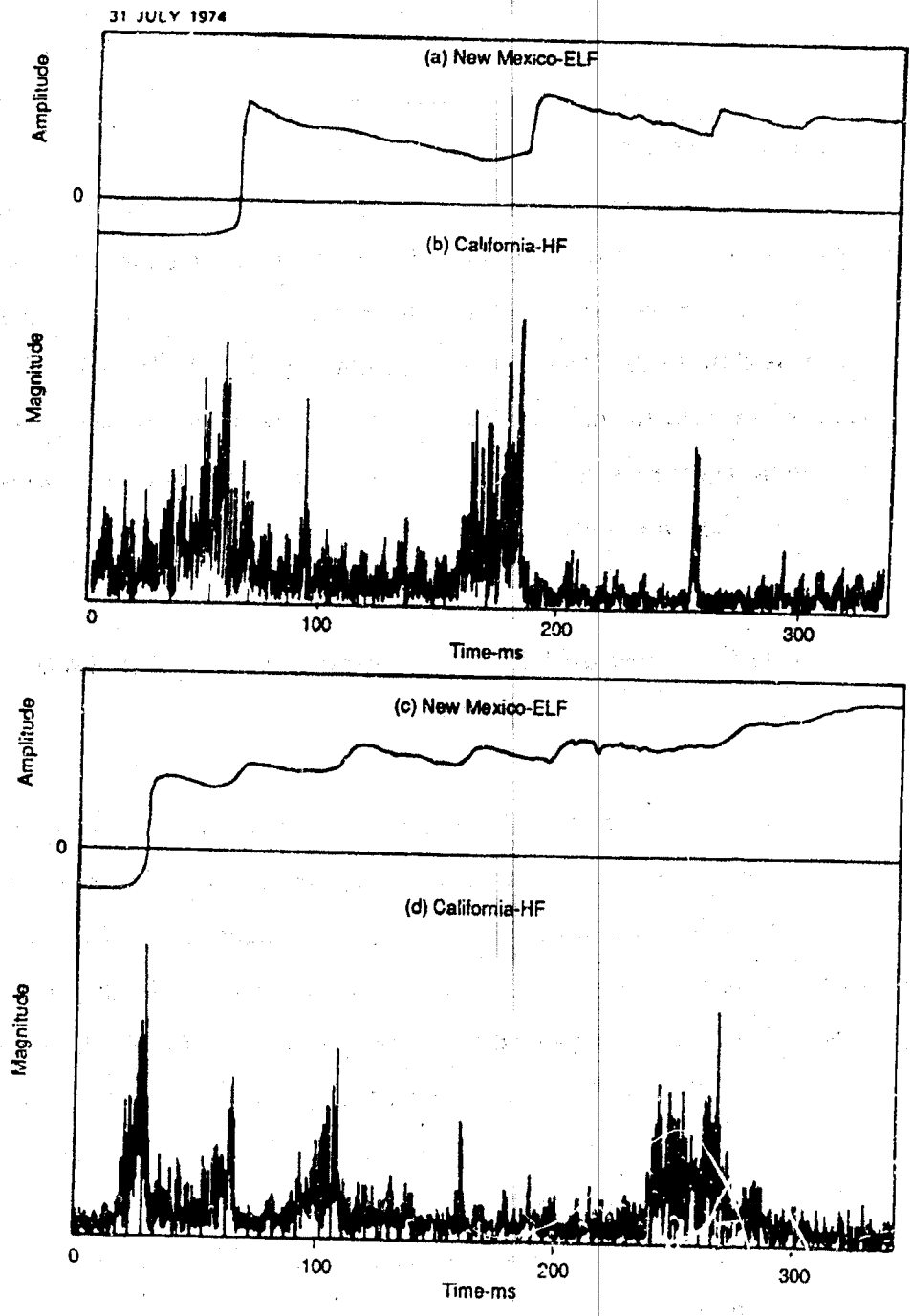

Figure 2-13. Atmospherics recorded simultaneously in New Mexico and California. Source Reference 2-22

which generally varies less than about 1-2 dB over periods of tens of minutes. Figure 2-14 shows a typical example of the short-term variability of the external noise on a CIT-to-CIT measurement basis. The observed noise levels (averaged over 2 minutes) are well within the expected bounds of the CCIR 322 predictions, as shown in Figure 2-15. For convenience, the rural man-made noise curve is also included. Other measurements indicate that the noise at frequencies which propagate to ranges of interest to OTH-radar operations is close to the atmospheric noise levels predicted. At higher frequencies, where galactic and man-made noise are the limiting noise types, the median noise observed at WARF from all sources was about 5 dB below the predictions for rural noise.

2.4.6 Noise Observed on Directive Antenna at WARF in 1986

When measured with WARF's highly directive receiving antenna array, external noise exhibits significant azimuthal dependence. The received transmitter-off noise level was frequently 3 to 5 dB higher in the eastward direction than in the westward direction. A nominal 8 to 10 dB difference in the noise level was also observed to the east when the array was steered from 70° to 120° T, with the higher levels occurring toward the southeast. A similar tendency (increasing noise levels when steered to the southwest) was observed with the array orientation the west (240° T to 300° T). Figure 2-16 shows the azimuthal dependence of noise measured on a WARF subarray. The whip noise, shown in Figure 2-17, was measured simultaneously with the data of Figure 2-16 and indicates no systematic time dependence. Hence, the changes shown in Figure 2-16 are the result of noise differences along the indicated bearings. The whip noise shown in Figure 2-17, when

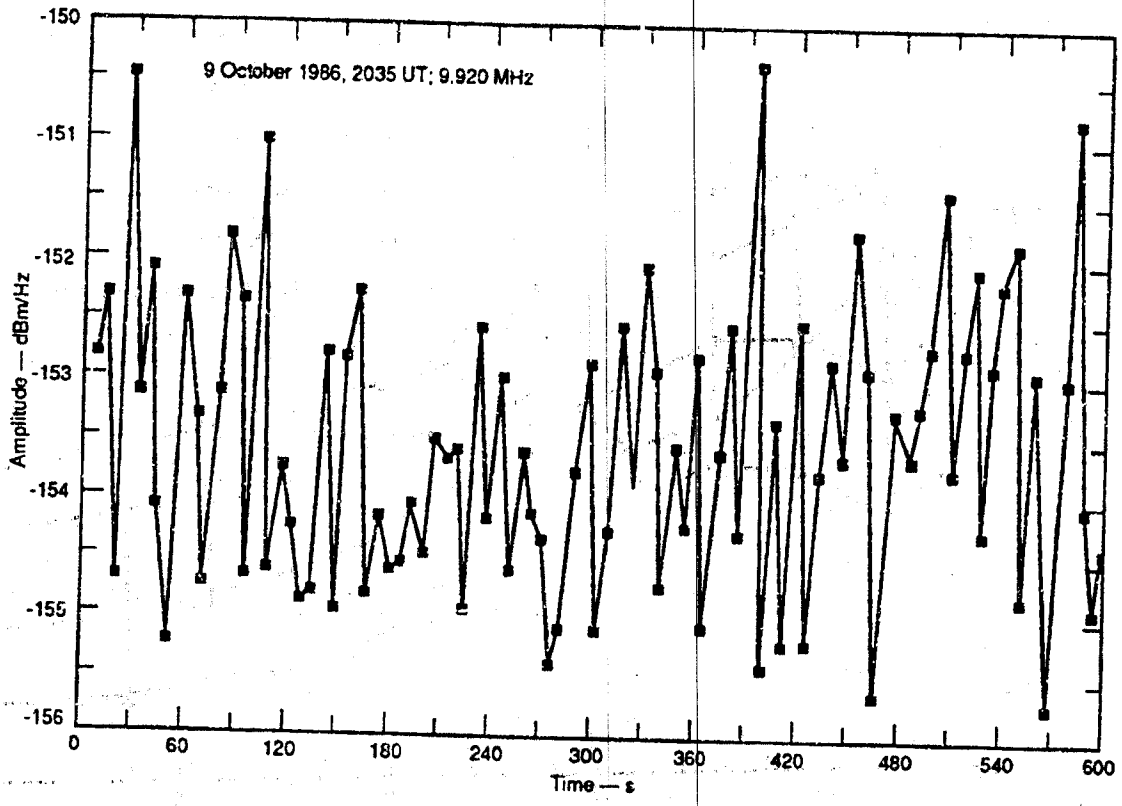

Figure 2-14. Time variation of noise observed on whip antenna.

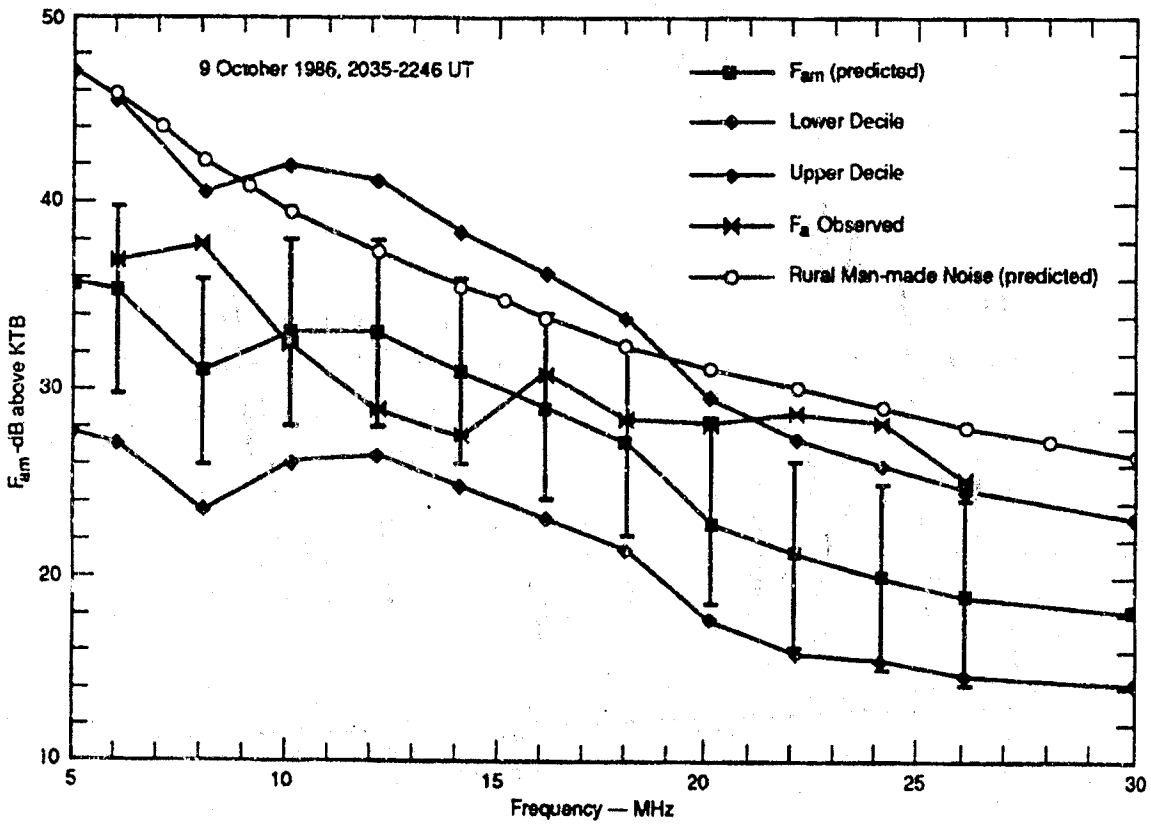

Figure 2-15. Noise vs. frequency observed at WARF on whip antenna compared to predictions.

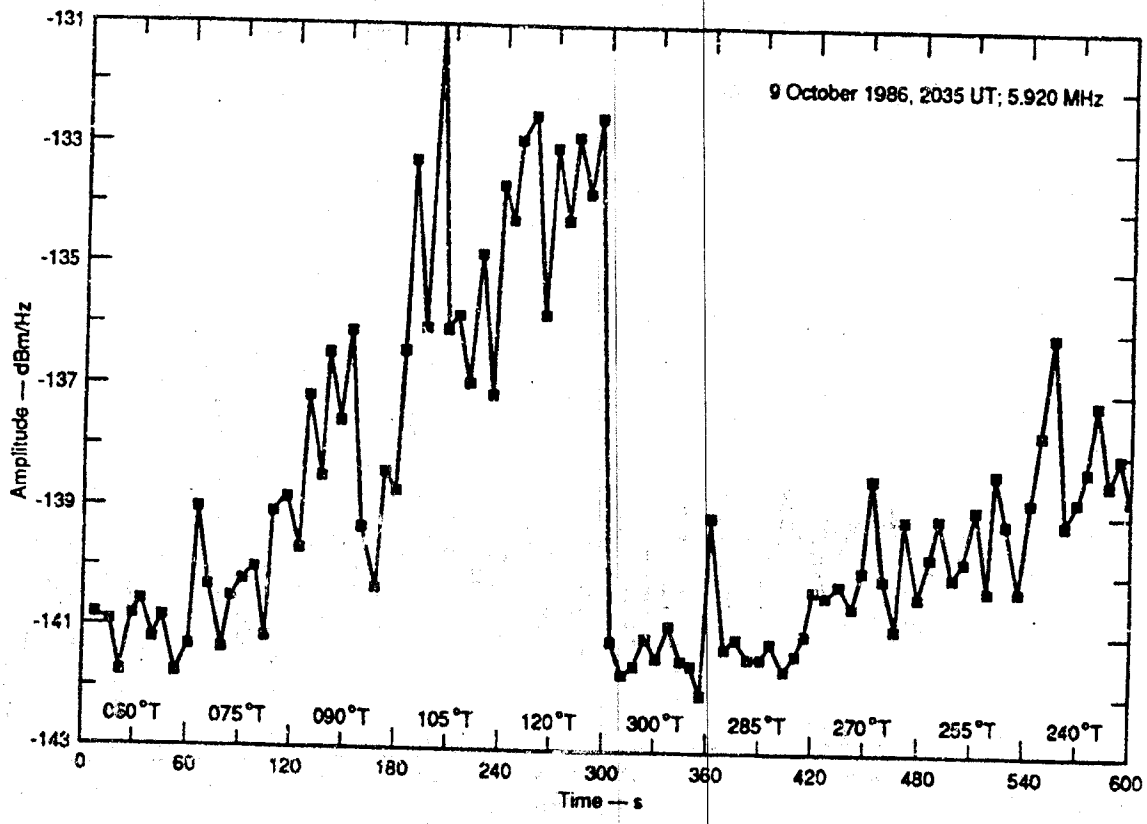

Figure 2-16. Azimuthal variation of noise observed from WARF on subarray.

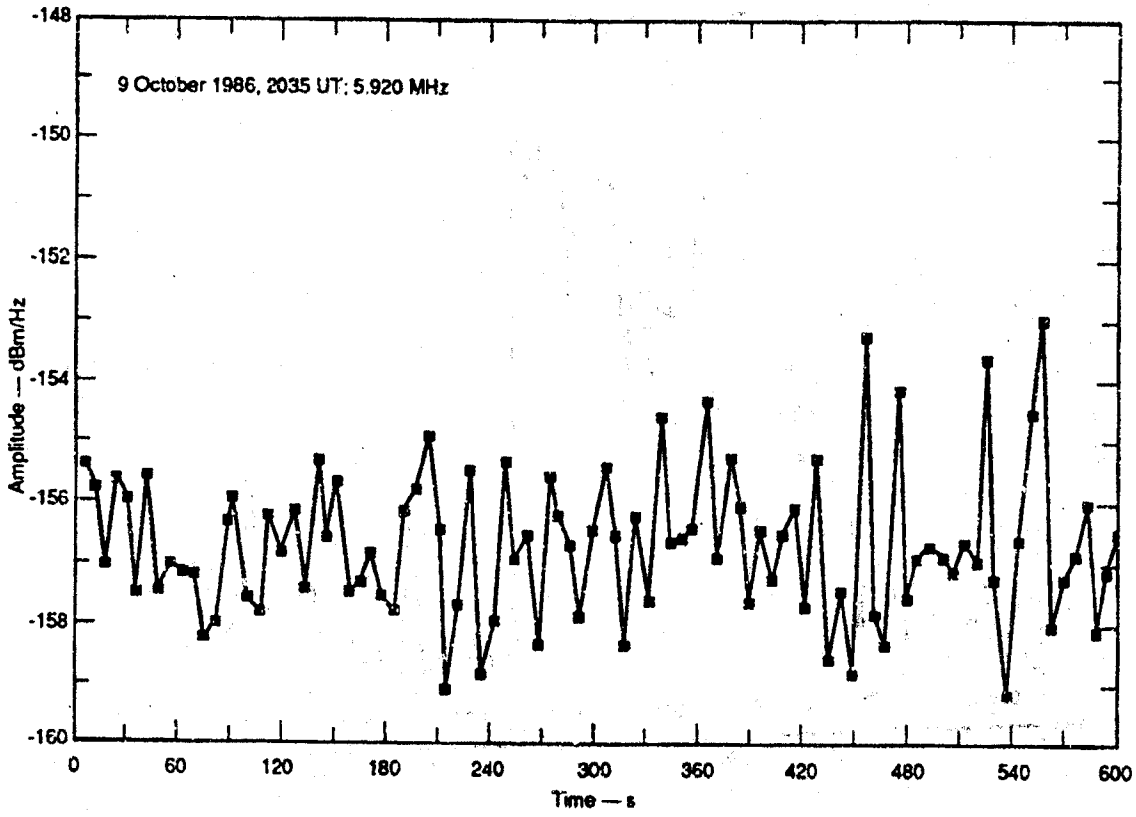

Figure 2-17. Noise observed from WARF on whip antenna.

corrected for feed and ground losses, is very close to the CCIR prediction for this season, time, and frequency. This is to be expected, since CCIR measurements were also made using a short vertical whip.

To summarize, the received external noise amplitude is generally Rayleigh distributed for each CIT. The CIT-to-CIT variation in RMS noise level is typically about 3 to 10 dB, while the RMS noise power versus time is log-normally distributed with a median value that generally changes little over several minutes. This is to be expected, since the integration time utilized for the CCIR 322 characteristics was four minutes.

2.5 Recommended Experimental Program

2.5.1 OTH Radar Facilities Available for Experiments

There are only a few dedicated experimental OTH radars in the continental United States: SRI International's WARF in central California, the Navy ROTHR site in Virginia, and a small OTH radar operated by Rome Air Development Center (RADC) near Verona, NY. At present, the Virginia ROTHR site is not functioning because the transmitting, receiving, and processing electronics are in use at the ROTHR site on Amchitka Island. However, the antennas and analysis facilities are operable and a replacement set of electronics is anticipated in the future. There are two operational or nearly operational OTH radar sites: the AN/FPS-118 in Maine and the ROTHR on Amchitka Island. While it is often difficult to conduct experiments at operational sites, the possibility should be explored, especially if the site has unique geographical or other advantanges.

2.5.2 Experiments for Existing and Future AOTH Test Beds

This class of experiments can be accomplished using existing OTH radar facilities, such as WARF, ROTHR in Virginia and/or Alaska, and the AN/FPS-118, as well as using a future advanced OTH ETB. In some cases experiments can be run using existing data tapes. WARF, ROTHR, and other OTH radars often record data in a manner which makes alternative processing possible, i.e., data are recorded at a relatively early, unprocessed stage. In the following discussion, we will group the experiments according to the issues addressed with relative priorities indicated. We have not stressed the issue of which facility is most appropriate for a given experiment. However, we do mention unique capabilities of various radars when they are pertinent to the experiment being discussed. Section 6 of Reference 2-4 makes suggestions for experiments to be carried out at specific OTH radars.

2.5.2.1 Residual Clutter Characteristics and Phenomenology

Importance of Residual Clutter

Doppler processing allows targets with doppler shifts greater than 1 or 2 Hz to be detected even though surface backscatter near "zero" doppler is some 10^6 times more powerful. Advanced OTH radar (AOTH) is required to detect small targets having signal strengths significantly less than 10^6 (60 db) below the zero-doppler surface return. Existing OTH radars experience a "clutter floor" which is spread in doppler, i.e., which exists at doppler shifts

of 5 to 10 Hz and more. The characteristics and phenomenology associated with this spread-doppler clutter are central to the effectiveness of advanced OTH radar because this clutter limits the small target detecting capability of AOTH. Below we discuss experiments to investigate and characterize residual spread-doppler clutter. In particular, we address two suspected mechanisms, meteor trail echos and round-the-world propagation paths.

Meteor Trail Echos

The mechanism by which meteor trail echos can cause spread-doppler clutter is discussed in Section 2.2.2 above. We think that investigation of this mechanism deserves top priority in AOTH experiment planning. There is significant evidence pointing to meteor trails as the primary components in residual doppler clutter and no experiment specifically addressing this critical point is yet in the planning stage — it should be. Identification of meteor trail echos requires a high resolution OTH radar since well known sources of spread-doppler clutter need to be avoided in order to observe the underlying residual clutter. The experiment design also needs to exploit the known characteristics of meteor trail echos (see Section 2.2.2 above and Reference 2-24). For example, meteor trail ionization occurs primarily at heights of 80 to 120 km so echos can be isolated spatially. Sporadic meteors occur with a known diurnal variation, the maximum rate occurring near 6 AM and minimum near 6 PM local time. Sporadic meteor rates during February are less than one-half those of July. There are meteor showers with greatly enhanced rates, e.g., the Perseid showers in August. A beginning for an experiment design could be to make OTH radar observations along azimuths and under operating conditions with customarily low spread-doppler clutter,

and see if the temporal variations expected from meteor trail echos occur. An example of meteor trail data was given in Figure 2-3.

Round-the-World Propagation Paths

RTW signals are another candidate mechanism for residual spread-doppler clutter. As discussed in Section 2.2.3 above, there are good reasons for thinking that signals transmitted by an OTH radar sometimes propagate around the world and enter the receive antenna from the back side. OTH radar antennas generally have a front to back ratio of less than 10 dB so signals on RTW paths have relatively easy access to the receiver. Experiments to investigate the RTW mechanism should have a high priority in AOTH experiment planning.

Experiments to investigate an RTW component in residual spread-doppler clutter can be done relatively easily with existing OTH radars. One approach would be to identify RTW echos by using appropriate waveforms and looking for echo powers at appropriate time delays, i.e., $\approx$ 140 ms and multiples thereof. Another approach would be to obtain the results quoted by McCrumb [Reference 2-23]. A third approach (not requiring an OTH radar) would be to use a rhombic antenna with an HF transmitter and receiver of appropriate type. The rhombic antenna is relatively high gain and can be reversed 180° in direction by simple switching. Hence a pulse could be transmitted in one direction and the antenna switched 180° specifically to receive the RTW signal.

Backscatter from Ionospheric Irregularities

Backscatter from ionosphere irregularities is known to produce spread-doppler clutter. For example, OTH radar is little used for observations into the earth's auroral zones because ionospheric irregularities are so common there. Also the polar magnetic field is more likely to be aligned perpendicular to the radar ray path and hence produce the conditions for magnetic-field-aligned irregularities which cause strong backscatter. Further, ionospheric irregularities move at velocities of tens of m/s and hence have significant doppler shifts, i.e., 1 to 10 Hz. Likewise, strong ionosphere irregularities occur near the equator. Fortunately, most OTH radar applications are at mid-latitudes, where irregularities occur less frequently and with less strength. Although backscatter from ionospheric irregularities has received considerable attention in the past, we think it still deserves a high priority in experiment planning for AOTH.

AOTH experiments should focus on residual clutter investigation related to mid-latitude irregularities in the main antenna beam well as clutter signals from auroral or equatorial irregularities that enter through range ambiguities and/or antenna side lobes. An interesting approach is suggested in Section 3.5 where a microwave radar is used to probe the ionosphere along the OTH radar ray path. The diagnostic information from the microwave radar would then be correlated with the OTH radar measurements of residual spread-doppler clutter to see if changes in ionospheric conditions could be related to changes in residual clutter. Further suggestions on experiments to isolate residual clutter sources into ionospheric and surface classes are discussed under clutter mapping below.

Backscatter from the Land and Sea

OTH radar returns from the land surfaces are fundamentally different than those from the sea. In both cases mechanisms have been suggested which might be capable of causing residual spread-doppler clutter. The AN/FPS-118 and ROTHR on Amchitka Island both observe areas mainly covered by ocean. WARF on the other hand can observe over both land and sea. As with ionospheric irregularities, land and sea clutter have been studied in the past. However, we think that further experiments deserve high priority because past work has not focused on the low-level residual clutter which is of particular interest here.

The sea surface moves constantly and hence the basic OTH radar return is spread in doppler. The two principal features are the Bragg lines spread from zero doppler by the frequency of the Bragg resonant ocean wave — usually 0.1 to 0.2 Hz. However, there are second and presumably higher order scattering effects which may contribute to spread-doppler clutter. Theoretical calculations according to the theory of Barrick could provide estimates for second-order backscatter. However, no high-order theory exits.

An initial approach to identify residual clutter from the sea would be to obtain range-azimuth doppler maps of sea clutter under conditions when known sources of spread-doppler clutter were absent. Comparisons of clutter maps and their time variations with maps of ocean-atmosphere measurements and their time variations should prove useful. Correlations of residual clutter with wind speed or wave height would indicate that higher-order ocean scatter is a likely mechanism for residual spread-doppler clutter over the ocean.

For the most part, land surface features do not move and hence to first approximation only a zero-doppler echo should appear. However, at the low signal levels corresponding to residual clutter uninvestigated mechanisms may come into play. For example, echos from regions with vegetation cover can be moved by the wind. Similarly echos from regions with road traffic are known to have spread-doppler echos. The observed doppler lines corresponding to Albuquerque freeway traffic are a well-known example. Another proposed mechanism is switching of electrical circuits. As with sea clutter, land clutter maps and their time variations can be compared with maps of relevant surface parameters and their time variations to look for correlations. Wind velocity, traffic patterns, and electrical use could serve as surface parameters to assess the mechanisms mentioned above.

Clutter Mapping

In the sections above we have suggested mechanisms which need investigation as possible sources of residual spread-doppler clutter. In many cases the spatial, temporal, and observation frequency variations of the clutter were suggested as means of identifying various mechanisms. Here we discuss clutter mapping, i.e., the use of time delay resolutions, antenna beam directionality, and observation frequency changes and time to "map" clutter variations. Another aspect of clutter mapping is to measure the correlation properties of clutter echos.

We think that clutter mapping plays an essential role in assessing the likely effectiveness of an advanced over-the-horizon radar in two ways. First, clutter maps are necessary to carry out the above recommendations regarding residual clutter characteristics and phenomenology. Second, the collec-

tion of an *appropriately guided* and comprehensive database for residual clutter should better establish the observational facts regarding residual clutter and thus allow better empirical and phenomenological understanding of this important limitation on AOTH radars. For these reasons we think clutter mapping should be given high priority in AOTH experiment planning.

Clutter maps: By *clutter maps* we mean a multi-dimensional database containing range-doppler maps of residual clutter power as observed by an OTH radar. In addition clutter variation, with azimuth, elevation angle, operating frequency, and time of observation, should be included where appropriate. The range-doppler map is only an example as azimuth, time of day, etc. could be used in place of the range variable depending on the type of investigation under consideration.

Advanced data manipulation and visualization techniques would be very useful in considering such a multi-dimensional database. For example, clustering algorithms could identify combinations of variables associated with high residual clutter levels.

The most general application of a clutter database is simply the empirical characterization of clutter. Given such a database, astute analysis would presumably discover interesting features that would lead to identifying residual clutter mechanisms. As discussed under techniques below, one of the primary goals of clutter observations would be to distinguish between clutter associated with surface scatter and that associated with ionospheric propagation. Such a distinction is very basic, but very useful and not well understood at present.

Basic clutter mapping techniques are simply to use the observational

capabilities of an OTH radar. For example, Figure 2-18 shows clutter power mapped as a function of doppler shift and range along a given azimuth beam for the ROTHR installed in Amchitka Island, Alaska. A number of targets are shown above the background clutter level. The single central peak identifies this observation as over a land surface. In this case the frequency resolution is about 0.1 Hz, and the range resolution (range bin size) is about 1.5 km.

Special techniques can be used to map clutter with higher resolution than can be achieved with existing radars. Existing antennas for OTH radars have fixed vertical beam patterns which are rather broad. Hence, ray peaks from virtually all elevation angles are accepted. To obtain resolution in elevation angle, some existing antennas, such as the WARF array, can be used in end-fire configuration, i.e., with the antenna beam pointed nearly along the array rather than the normal case of near perpendicular to the array length. Elevation angle resolution of some 2° to 3° can be obtained in this way to study clutter variations with elevation angle. In some cases this resolution should be good enough to separate different ionospheric propagation modes.

Transponders can be useful in that they can provide a target signal not influenced by the surface conditions. Thus, returns from a transponder are primarily affected by ionospheric propagation rather than surface activity. Similarly, one-way transmission from a small source in the target area can be used to differentiate between clutter introduced by ionospheric propagation and clutter due to the surface scattering process.

WARF and ROTHR use twin-whip (TWERP) antennas in the receive array. By reversing the phasing on these TWERP antennas, the array can be directed to either side of the array length. Thus, the WARF system in central California can look either east over the southwestern United States to

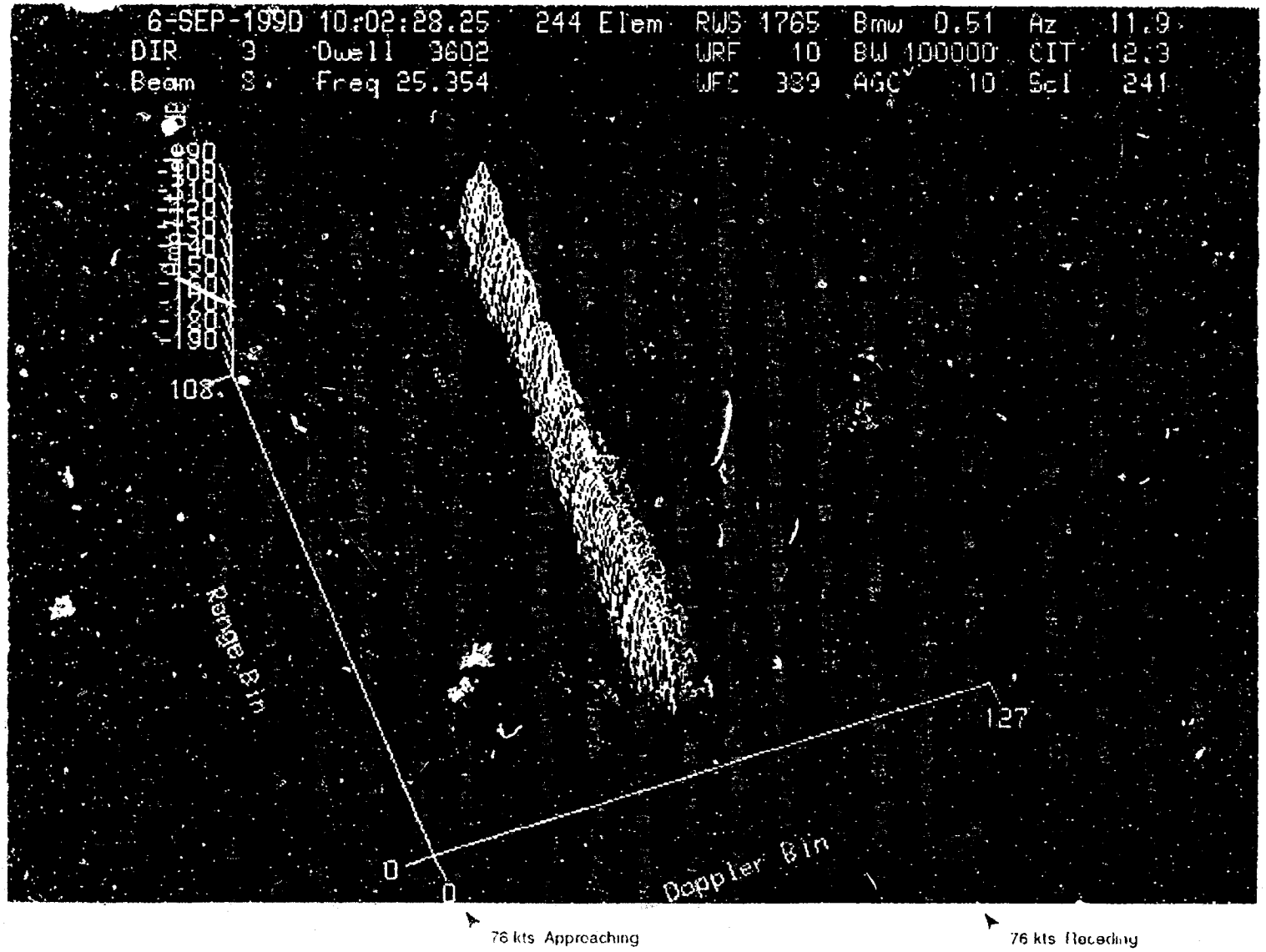

Figure 2-18 Range doppler clutter map collected by ROTHR at Amchitka Island during September 1990. Note that the central "zero" doppler peak is shifted off zero by ionospheric motion. The small red topped peaks away from the larger central peaks are targets, while the blue or green background is clutter from the land surface in the field of view of the radar.

THIS
PAGE
IS
MISSING
IN
ORIGINAL
DOCUMENT

observe ground clutter or west over the Pacific Ocean to observe sea clutter. ROTHR as presently configured on Amchitka Island looks southwest. The receive antenna array could be reversed to look northwest toward the auroral zone, but the transmit antenna can only look southwest. When a second new ROTHR set of electronics is installed at the Virginia site, thought should be given to providing a north-looking capability as well as the current south-looking capability.

Here we have only briefly sketched techniques for clutter mapping. Reference 2-4 discusses a number of techniques in detail with recommendations for specific radars.

2.5.2.2 Ionospheric Propagation Characteristics and Phenomenology

Radio amateurs and shortwave listeners are familiar with the fluctuation of amplitude and phase impressed upon HF radio signals propagated via the ionosphere. These fluctuations in amplitude and phase, and their variations over time, space, bandwidth, and operating frequency limit the performance of OTH radars and can contribute to residual spread-doppler clutter. It is important for the assessment of AOTH radar potential to understand these limitations and sources of ionospheric clutter. A good understanding of such problems enables us to estimate their limitations and to try to mitigate them by proper radar design. In the sections below, we discuss experiments related to coherence, one-way transmissions from small transmitters, and the excitation of ionospheric instabilities by very high transmitter power levels.

Signal Coherence Experiments

The term *signal coherence* encompasses several effects related to signal coherence in time, space, and bandwidth. *Time coherence* refers to the length of time an ionospheric propagation path remains stable in amplitude and phase. The coherent integration time used by the radar must be less than the coherence time of the ionosphere to allow the doppler-shifted components of the echo signal to be placed in the proper doppler bin. The longer the CIT, the finer the doppler resolution. *Spatial coherence* refers to the area on the earth over which one can move a receiver and still have stable amplitude and phase for an ionospherically propagated signal. This factor is important because it limits the size of the antenna that can be used. The antenna must be smaller in length, width, and height than the coherence volume for the propagation path in use. Signal coherence also limits the signal bandwidth that can be used and hence the range resolution. If coherence (stable amplitude and phase) can be maintained over a given band of frequencies then echo signals will be placed in the proper range bin. The wider the *coherent bandwidth*, the finer the range resolution. For example, a 100 kHz coherent bandwidth allows 1.5 km range resolution while a 1 MHz coherent bandwidth allows 150 m range resolution. As range resolution becomes finer, new applications for OTH radar can be considered.

It is clearly a high priority for AOTH radar development to have a good working knowledge of the time, space, and bandwidth coherence of ionospheric paths and how these quantities vary with time, observational geometry, and other radar parameters. Such knowledge is important in two ways. First, knowledge of signal coherence determines limits on an OTH radar's range, doppler, and azimuth resolution. Second, knowledge of signal

coherence characteristics may allow discovery and development of techniques to correct for ionospheric distortion and extend effective coherence in time, space, and bandwidth.

Basic signal coherence experiments add sample OTH radar signals over one-way or two-way paths using signal sources in the "target" area for one-way measurements or transponders for two-way measurements. While basic work is needed understanding time, space, and bandwidth coherence over a wide range of ionospheric conditions and radar parameters and locations, we think that some focused experiments have high priority so that the following issues can be addressed.

- What is the maximum practical size for an AOTH radar in terms of spatial coherence?
- What is the maximum practical bandwidth in terms of frequency coherence?
- What is the maximum practical CIT?

Resolution of these issues determines the best practical range, azimuth, and doppler resolution of an AOTH radar, and hence the types of applications for which it can be used. Some example experiments are discussed below.

Ionospheric dispersion generally limits the coherent bandwidth that can be used. Interference is another limitation as discussed below. Experimental evidence suggests that ionospheric dispersion can be corrected to some extent and that coherent bandwidths of $\sim$ 1 MHz might often be made available using corrective schemes. Parent and Bouodillion [Reference 2-25] suggest

other correction methods for HF radars. We recommend one-way and two-way experiments to both measure coherent bandwidth and test dispersing correction techniques. We point out that bandwidths of 1 MHz may make practical the resolution of multiple bounce signals between aircraft targets and the surface and hence allow estimates of aircraft height. At the present time, to our knowledge, only WARF has the capability to process 1 MHz bandwidth signals.

One-way Experiments

One-way experiments involve a small source in a "target" region and propagation to the OTH radar receive antenna. The OTH radar transmitter is not used. This technique can eliminate surface scattering, and hence focus attention on the ionospheric transmission path to explore sources of ionospheric clutter and other limitations imposed by the ionosphere. One basic experiment is to transmit a monochromatic CW signal and observe the phase and amplitude fluctuations imposed by the ionosphere. The monochromatic signal is usually doppler broadened, providing a measure of spread-doppler clutter introduced by ionospheric propagation.

Another interesting experiment involves using an antenna with some antenna resolution in elevation. For example, a long array such as WARF could be used in end-fire configuration to obtain $\sim 2°$ to $3°$ of resolution in elevation. Experiments could be done to investigate the separation of ionospheric propagation modes, e.g., high-ray and low-ray, and thereby possible reductions in spread-doppler clutter.

Further experimental recommendations for experiments on specific radar are given by Reference 2-4, Chapter 6.

Excitation of Ionospheric Instabilities by High Power

In Section 2.3, we examined an interesting situation with regard to the generation of ionospheric irregularities induced by high-power OTH radar transmissions. Such irregularities are likely to induce phase and amplitude fluctuations on signals propagating through them. If generation of such irregularities is indeed confirmed for projected power levels for AOTH radars, then experiments, such as the one-way transmission discussed above are recommended to observe the effects of these irregularities in terms of signal distortion and the introduction of spread-doppler clutter.

2.5.2.3 Noise and Interference Characteristics and Phenomenology

Noise, mainly impulsive noise from distant and local lightning, and interference, mainly from other HF spectrum users, limit OTH radar performance. Estimates of the limitations imposed by noise and interference are somewhat uncertain and should be classified to properly assess AOTH performance projections. Existing noise surveys at HF [Reference 2-19] are deficient in several ways, in particular impulsive noise is averaged over 200 s and an isotropic antenna is used for data collection. We recommend experiments directed at collection of noise statistics more relevant to AOTH radar and correcting the drawbacks of CCIR Report 322 [Reference 2-19]. Noise measurements using the same techniques as CCIR should also be made for comparison. A technique demonstration suggested below could include noise measurements.

Measurements of noise and interference should include high resolution in both space and time, i.e., variations with antenna azimuth (and elevation) are important, as are measurements of impulsive noise. Impulsive noise is important because it creates a "noise floor" of spread-doppler clutter. Noise and interference statistics and their variations with time, direction, radar parameters, etc. should be measured. We point out the many hours of data collected on tape by ROTHR, WARF, and other radars which could probably be used in noise and interference surveys. We recommend that these sources of data be considered before further field experiments are made.

2.5.2.4 Technique Demonstrations

In addition to the somewhat basic experiments described above, we recommend technique demonstrations. An example concerning noise mitigation is suggested below.

Noise Mitigation Demonstration

There are two levels to this experiment. The first level and the less difficult of the two is time domain exclusion of impulsive events. The idea would be simply to edit the data to exclude the time interval during which a strong impulsive noise signal occurs. For example, lightning strokes within $\approx$ 2,000 km of the receive site would constitute strong impulsive noise which could well be successfully edited. Auto ignition noise would be another example. The nature of impulsive noise suggests that wavelet transform processing could be useful.

The second level is probably more difficult. This experiment would be to put antenna pattern nulls on impulsive noise sources using adaptive beam forming. The technique of adaptive beam forming for mitigation of man-made interfering signals has been explored by Washburn and Sweeney and is reviewed in Kolosov et al. [Reference 2-26]. However, it has not, to our knowledge, been used to mitigate lightning noise. A simple version of the idea would be to form a simple adaptive OTH radar antenna by the introduction of "side-lobe cancelling" elements, either from the array itself or by using additional antenna elements. This simple adaptive array would then be used to implement adaptive beamforming for suppression of impulsive noise. The results of this simple pilot experiment could be used to guide more ambitious experiments with the more capable antenna proposed for the advanced OTH ETB.

REFERENCES

2-1. Eshleman, V. R., P. B. Gallagher, and A. M. Peterson, "Continuous Radar Echoes from Meteor Trails," *Proc. I. R. E.* 43, p. 489 (1955).

2-2. Thomas, R. M., P. S. Whitman, and W. G. Elford, J. Atmospheric and Terrestrial Phys. 50, 703 (1988).

2-3. Eshleman, V. R., "Meteor Scatter," Scientific Report No. 4, Stanford Electronics Laboratories, Stanford, CA, August 1958.

2-4. Cornwall, M., S. Drell, W. Happer, R. Lelevier, G. MacDonald, A. Peterson, S. Ride, J. Sullivan, and J. Vesecky, "OTH for Verification (U)," JASON Report No. JSR-90-850, (The MITRE Corporation, McLean, VA, 1990).

2-5. Gurevich, A. V., and E. E. Tsedilina, "Long Distance Propagation of HF Radio Waves," Spinger-Verlag, Berlin (1985).

2-6. Fenwick, R. B., "Round-the-World High Frequency Propagation," SEL Tech. Rpt. 71, Radioscience Lab., Stanford University, Stanford, CA (1963). Fenwick, R. B., "Sweep-Frequency, Spaced-Station Measurements of Round-The-World HF Propagation," SEL Tech. Rpt. 122, Radioscience Lab., Stanford Univ., Stanford, CA (1966).

2-7. Fenwick, R. B., and O. G. Villard, Jr., "Measurements of the frequency dependence of round-the-world HF pulse time delays and dispersions," *Proc. IEEE*, 51, 1240 (1963).

2-8. Barker, J. I., and M. D. Grossi, "Results of the OV-4 Dual Satellite Experiment on Guided Ionospheric Propagation," *Radio Sci.* 5 983 (1970).

2-9. Elkins, T. J., "Clutter Model for OTH Radar," MITRE Report MTR 10299, August 1987.

2-10. Franchi, P. R., and E. J. Tichovolsky, "Phase Screen Modulation as a Source of Clutter Related Noise in Over-the-Horizon Radars," Rome Air Development Center Report RADC-TR-89-296, November 1989.

2-11. Argo, P., J. Fitzgerald, and R. Carlos, "NICARE-I HF Propagation Experiment: Results and Interpretation," Radio Science 27, 299 (1992).

2-12. Utlaut, W. F., et al., "Some ionosonde observations of ionspheric modification by very high power high-frequency, ground-based transmission" *J. Geophys, Res.* 25, 6429 (1970).

2-13. Thome, G. D., and F. W. Perkins, "Production of ionospheric striations by self-focusing of intense radiowaves," *Phys. Rev. Lett.* 32, 1238 (1974).

2-14. Perkins, F. W., and E. J. Valeo, "Thermal self-focussing of electromagnetic waves in plasma," *Phys. Rev. Lett* 32, 1234 (1974).

2-15. Duncan, L. M., and R. A. Benke, "Observations of self-focussing electromagnetic waves in the ionosphere," *Phys. Rev. Lett.* 41, 998 (1978).

2-16. Perkins, F. W., and M. V. Goldman "Self-focusing of radiowaves in an underdense ionosphere," *J. Geophys. Res.* 86, 600 (1981).

2-17. Novozhilov, V. I., and S. M. Savel'yev, "Irregular structure of the ionosphere in a field of a strong obliquely incident radio wave," *Geomagnetism and Aeronomy* 18, 145 (1978).

2-18. Gurevich, A. V., *Nonlinear Phenomena in the Ionosphere*, p. 5. Springer-Verlag, New York, (1978).

2-19. CCIR Report 322, "World Distribution and Characteristics of Atmospheric Radio Noise," International Telecommunication Union, Geneva (1964).

2-20. Horner, F., "Radio Noise from Thunderstorms," *Advances in Radio Research*, J. A. Saxton, ed., Vol. 2, pp. 121-204 (Academic Press, London, 1964).

2-21. Oetzel, G. N., and E. T. Pierce, "The Radio Emissions from Close Lightning," Scientific Note 10, Contract NONR-4099(99), NR 082-206, Stanford Research Institute, Menlo Park, California (1968).

2-22. Zavoli, W. B.,"Observed Characteristics of Ionospherically Propagated HF Atmospherics from Normal and Severe Thunderstorms," Ph.D. Dissertation, Stanford University (May 1977).

2-23. McCrumb, J. B., "Residual Clutter and Noise Effects on OTH Radar Performance," SRI Project 2161, Contract N0-0014-86-C-0406, SRI International, Menlo Park, California (April 1989).

2-24. Davies, K., *Ionospheric Radio Propagation*, National Bureau of Standards Monograph 80, Chapter 8, U.S. Government Printing Office, Washington, D.C. (1965).

2-25. Parent, J., and A. Bouodillion, "A method to correct HF skywave backscattered signals for ionospheric frequency modulation," *I.E.E.E. Trans. Antenna and Propagation*, AP-36, 127-135 (1987).

2-26. Kolosov, A. A., et al., *Over-The-Horizon Radar* (translated from the 1984 Russian Edition by W. F. Barton), Artec House, Boston (1987).

3 HOW CAN WE LEARN THE MOST FROM THE EXPERIMENTAL TEST BED?

3.1 AOTH as a Multi-Mission Capability

Defense policy and planning in the United States is currently undergoing major restructuring in recognition of a dramatically altered international situation. Because of this, it is more important than ever that military R&D programs and facilities be designed and operated as true experimental facilities in order that they may efficiently serve the widest possible set of current and future needs. Given the inherent unpredictability of the future, this can only be achieved if these facilities are flexible in design and are conceived as multiple-year research efforts that are not rigidly tied to currently perceived operational requirements. Otherwise, R&D funding will be wasted on narrow efforts of transient importance, as has sometimes been the case in the past. Support for OTH radar research should be viewed in accord with these principles.

In particular, although the current justification for an AOTH program is cruise missile detection in the context of the Air Defense Initiative, this motivation should not dictate all aspects of the proposed research facility. Clearly, long before an AOTH experimental facility could be completed and exploited ,and follow-on operational OTH units developed as part of an air defense system against Soviet cruise missiles, the nature of the current threat may change dramatically for the better, e.g., by virtue of arms control agree-

ments with the Soviet Union, or the worse, e.g., by virtue of the spread of cruise missile technology to other countries or the widespread use of low-observable technologies. Thus, it is important to view any AOTH research program broadly.

3.2 Multi-Mission Perspective for an AOTH Facility

The proposed AOTH effort needs to be considered as more than a tool to answer the specific question of whether OTH radars can detect individual cruise missiles. Rather, the goal of an OTH research program should be to answer a fundamental question that has existed since the 1970s, namely what limits to sub-clutter visibility of OTH radars are set by the characteristics of the ionosphere and other natural phenomena. This question was raised by the dismal performance of the FPS-95 OTH radar that was once deployed in England but subsequently abandoned. The answer to this fundamental question remains elusive in spite of much that has been written and learned since the 1970s.

Cruise missiles are clearly an important target for any OTH research program. Other tasks of national importance for which OTH research data are needed include: the limits of OTH radars for the detection of large and medium-sized aircraft (whether they are cruise missile carriers or aircraft carrying illicit drugs into the United States); the possibility of improved detection of all sizes of ships in various sea states; possible applications to the verification of arms control agreements limiting rail- and road-mobile missile

carriers [Reference 2-4]; capability of detecting the mobilization of conventional armed forces; and specialized intelligence missions. Other applications will surely be suggested in the future.

The optimal siting of the experimental OTH facility needs to keep in mind the above spectrum of potential missions as well as the fundamental technical issues that need to be explored in a multi-year experimental program to determine the limits set by nature to OTH radar performance. In particular, the radar needs to be sited so that it can view targets over land as well as sea. It needs to be able to view areas where the United States test flies ALCMs and SLCMs, since tests that require specially procured targets inevitably become expensive and consequently occur all too infrequently. For the same reason, the facility should be positioned to view areas that have substantial commercial and military air traffic, ship traffic, and train and truck traffic. Although WARF's location makes it impossible to observe the U.S. cruise missile test ranges at Eglin, AFB and Pt. Magu, this facility can view many other types of targets and in doing so has repeatedly proven the value of being able to take data on targets of opportunity.

Although it may not be possible to find a site that can view all of the types of activity listed above, thoughtful compromises should be chosen in order to keep the spectrum of potential targets as broad as possible. For example, it might be better to retain just the most active of the two U.S. cruise missile test areas in the field-of-view since ALCMs and SLCMs have

comparable radar cross sections and other characteristics, rather than picking a site that, say, excludes coverage of an interesting class of targets that move on land.

Another consideration in siting is the desirability of being at a location that uses parts of the ionosphere that can be viewed by other means, e.g., by high frequency radars such as Millstone Hill in Massachusetts.

The AOTH radar should be conceived as an incremental design with equipment upgraded over a multi-year period, as lessons are learned from experimental operations and the most important parameters identified for upgrading performance. This would serve better in the long run than a rigid design optimized to today's understanding and hardware, because an incremental approach would produce data sooner, would be cheaper initially and less likely to experience cost and schedule overruns, and because it would be more flexible and therefore actually more economic in the long run.

Important capabilities that need to be explored in a U.S. experimental OTH radar program include: quantitative improvements that derive from an ability to form narrow beams in elevation and azimuth, the performance of unfilled arrays and comparison with theoretical expectations, and data gathered over a much larger range of ionospheric conditions so that meaningful statistics can be compiled. Also, quantitative study of meteor effects, atmospheric heating at high-power operations, and adaptive nulling of noise sources in the field of regard of the radar are topics that need quanitative study with an advanced research facility.

Happily, essentially almost all of the above items are in the plans for the AOTH as currently conceived. What seems to be missing, however, is the realization that resolving the list of fundamental issues will be a multi-step process with occassional trips up blind alleys and the need to regroup and come up with new approaches. It is simply impossible to specify a master schedule now and expect that progress will be orderly and programmable.

3.3 The Experimental Planning Process

An important way to clarify the choice of hardware priorities (size, power, number of beams) for the ETB is to begin with a clear statement of the main scientific experiments that would be done on the ETB facility during the first several years. Although we were told that DARPA has established a committee to study possible experiments for the ETB, we are concerned that, because of its size and structure, it may not be well enough focused to produce a short, prioritized list within a reasonable time period. We therefore recommend that DARPA either re-configure this committee or establish a new, smaller working group to develop a first-cut experimental plan now. From this strawman experimental plan will emerge a more realistic assessment of the design requirements for the ETB facility. In Section 2.5 above, we have presented a few of our own ideas for experiments.

After the first-cut, prioritized experimental plan is in hand, it will be easier to assess whether a large, expensive ETB is critical to performing the highest priority experiments for AOTH development.

3.4 Side-Lobe Power versus Main-Beam Power

A key feature of the ETB facility is the use of a sparsely filled array to achieve narrow beam patterns. But in a sparsely filled array only a small fraction of the power is transmitted in the main beam: almost all the power goes into side lobes. The reciprocal principle applies to receive beams; if the beam were viewing an extended object, then almost all the power entering the receiver arrives from side lobes.

It follows that there is a critical degree of sparseness below which an OTH would be principally viewing side lobes rather than main beams. Antenna designers should present calculations that demonstrate that in the most relevant two-way paths, the dominant signal is the main beam signal. It does not suffice that the peak gain exceeds side lobe gain by a factor N — the number of elements. This is true regardless of sparseness. If the array is very sparsely filled, then the main beam is *narrow* and contributes negligably to the total transmitted power. One must compute the integrated gain product

$$< G^2 >= \frac{1}{4\pi} \int d\theta \cos\theta d\theta \, G_T(\Theta,\theta) \, G_R(\Theta,\theta)$$

and demonstrate that the principal contribution arises from the main beam. Here Θ denotes elevation angle, θ the azimuth angle, and G_T G_R the transmit and receive gain functions, respectively.

3.5 Ionospheric Diagnostics in Conjunction with the ETB

3.5.1 Introduction

In Section 2.2, we discussed possible causes of residual spread-doppler clutter. Propagation through and scattering from ionospheric inhomogeneties play an important role as candidate mechanisms for residual clutter. Investigations of ionospheric clutter mechanisms would be greatly aided by diagnostic measurements of the ionosphere through which the OTH radar waves propagate. For approximately the last 30 years, VHF/UHF ionospheric radars have made such measurements. [Reference 3-1]. We strongly recommend using ionospheric diagnostic measurements by up-looking microwave radars, such as Millstone Hill in Massachusetts, in conjunction with residual clutter measurements by OTH radars, to investigate ionospheric causes of residual spread-doppler clutter.

3.5.2 Ionospheric Radar Locations

Microwave ionospheric radars are currently located along an approximately north-south belt from Areceibo in Puerto Rico to Millstone Hill in Massachusetts to Sondre Stromfjord on the west cost of Greenland. These

locations are shown in Figure 3-1. There are also similar ionospheric radars in Norway (ISCAT) and in Peru at Jicamarca.

3.5.3 Operation and Capabilities of Ionospheric Radars

Ionospheric radars operating at frequencies from 46.5 MHz (MO, Japan) to 1,290 MHz (Sondre Stromfjord) depend on backscatter at frequencies well above the ionospheric plasma frequency. Two scattering mechanisms are involved, namely incoherent scattering from individual electrons (Thompson scatter) and coherent scatter from electron density fluctuations of the order of the radar wavelength. By a variety of measurement techniques, including the examination of the doppler spectrum of the backscattered radar waves, these ionosphere radars can estimate a number of interesting and relevant ionosphere plasma characteristics. These characteristics are summarized below for E and F region measurements:

- Electron density
- Electron and ion temperatures
- Ion velocity
- Ion-neutral collision frequency (E-region only)
- Ion composition (F-region only)
- Strength of electron density fluctuations on size scales comparable to one-half the radar wavelength

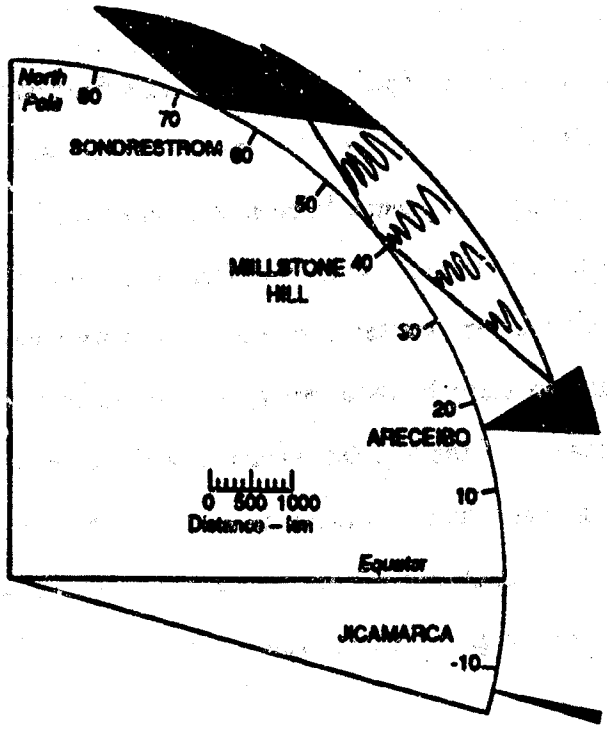

Figure 3-1. Vertical plane coverage of VHF and UHF ionospheric radar deployed north to south along a belt of longitude from 50° to 80° W. longitude.

These measurements can be made at ionospheric heights of from 90 to 1,000 km depending on the field of view of a given radar. The geographical coverage of an ionospheric radar is limited both by its antenna and the observational geometry. In Figure 3-1 we see the coverage of three ionospheric radars in the vertical plane. The Areceibo radar has a large fixed antenna that can be scanned over a limited range of angles near vertical, but cannot point toward the horizon. The Millstone Hill and Sondre Stromfjord radars have large parabolic dish antennas which can be pointed nearly toward the horizon. The coverage of these radars in range runs from 100s to about 1000 km from the radar, depending on the ionospheric height being probed.

3.5.4 Use of VHF and UHF Ionospheric Radar in Clutter Research

The basic idea is to map ionospheric quantities of interest near the OTH radar's mid-path point using the ionospheric radars shown in Figure 3-2. The results of the ionospheric radar diagnostic measurements would be used in conjunction with OTH radar residual clutter measurements to investigate clutter mechanisms related to the ionosphere. For example, the ionospheric instabilities which may be excited by high OTH radar powers (see Section 2.3) could probably be observed using one of the ionosphere radars shown in Figure 3-2. A basic investigation would initially move along empirical lines noting changes in ionospheric characteristics with time and then looking for correlated changes in clutter measurements. When ionospheric sources of

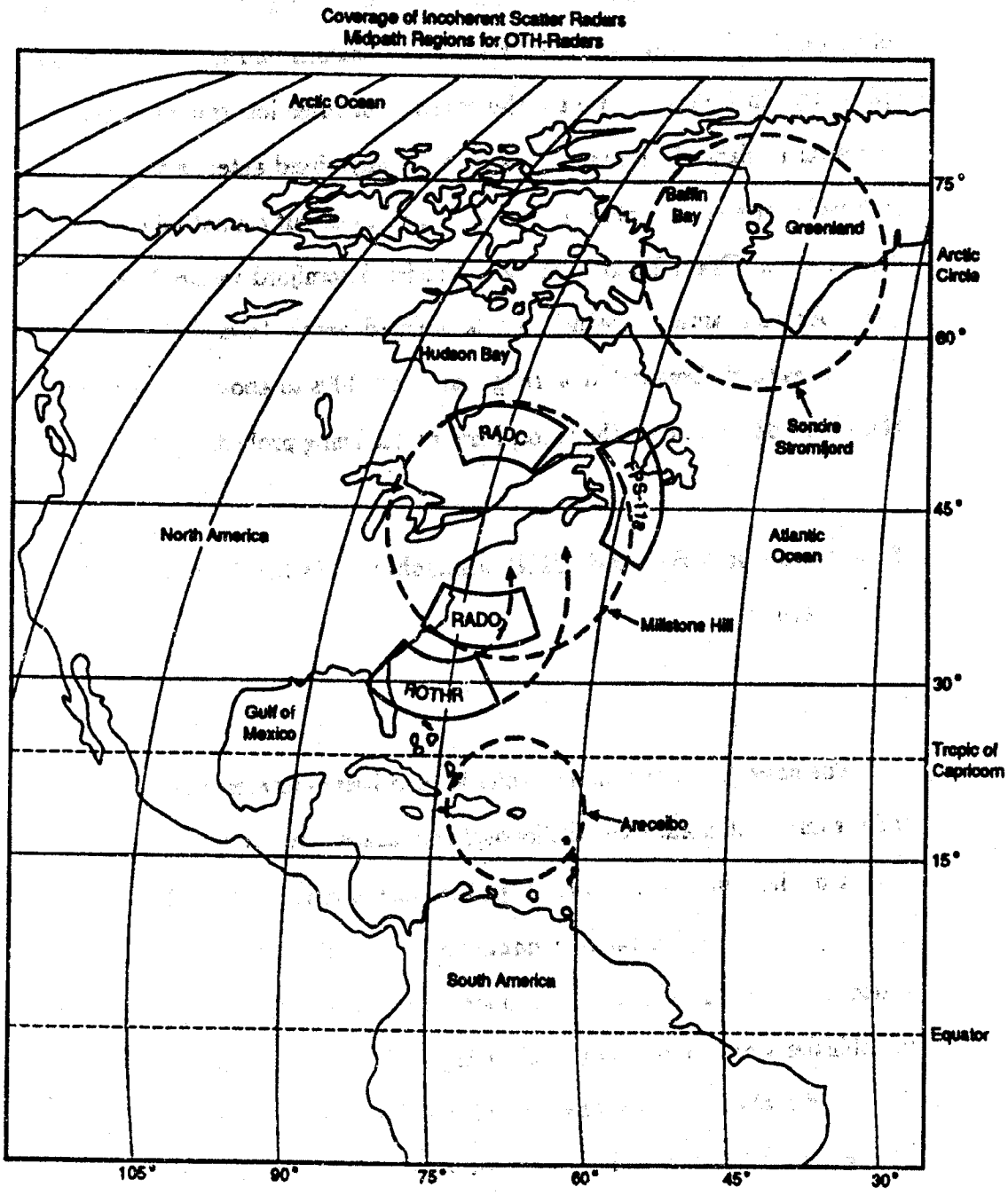

Figure 3-2. Coverage of ionospheric VHF and UHF radars (dashed circles) compared to mid-path regions for existing and projected OTH radars. The range coverage for the ionospheric radars is for a 300 km ionospheric height.

clutter become better understood, ionospheric radars can provide estimates of ionospheric plasma parameters which will be necessary in evaluating and applying quantitative models of ionospheric clutter.

3.5.5 Geographic Aspects of Using Ionospheric and OTH Radar Together

To use ionospheric VHF and UHF radars in conjunction with OTH radars in residual clutter (or other AOTH) experiments, it is necessary that the mid-path region for the OTH radar be located within the coverage area of an ionospheric radar for the relevant ionospheric heights. Figure 3-2 shows the locations of the Sondre Stromfjord, Millstone Hill, and Areceibo radars and their approximate coverage ranges for an ionosphere height of 300 km. Also shown are the approximate mid-path regions for three nearby OTH radars, namely the AN/FPS-118 located in Maine, the Rome Air and Development Center radar at Verona, NY, and the ROTHR site in Virginia.

As the Figure 3-2 shows, the Sondre Stromfjord and Areceibo ionospheric radars are not relevant at the present time. The Millstone Hill radar has useful coverage over the RADC OTH radar mid-path region and possibly the AN/FPS-118 mid-path region as well. The ROTHR mid-path points for the current configuration (south looking) are mainly outside Millstone Hill coverage. However, if ROTHR were augmented to look north or, better still, to look to the east and southeast, Millstone Hill could achieve good coverage. Similarly if the AN/FPS-118 could be augmented to look west or southwest

its mid-path points would be within Millstone Hill coverage. Probably, the best plan given that the AN/FPS-118 is an operational site and that the ROTHR Virginia site is experimental, would be to augment the Virginia ROTHR site with the necessary antenna to extend northeast-to-southeast into the southeastern sector of the Millstone Hill radar coverage.

Clearly the discussion above constitutes only an idea with useful possibilities. We recommend further investigation and evaluation of using ionospheric diagnostics from the Millstone Hill radar in conjunction with OTH radar observations of residual clutter. Such a combination is likely to produce very useful results regarding residual clutter characteristics and mechanisms, as well as useful information regarding OTH radar performance in general.

REFERENCE

3-1. Kelly, M. C., *The Earth's Ionosphere: Plasma Physics and Electrodynamics*, Appendix A, (Academic Press, San Diego, 1989).

4 REDUCTION OF HF RADAR CROSS SECTION FOR CRUISE MISSILES

4.1 Cross-Section Reduction

Methods for the reduction of radar cross section have been discussed in the open literature for many years. Here we summarize some information from the 1970 edition of *the Radar Cross Section Handbook*, Vol. 2, edited by G.T. Ruck, a widely available reference [Reference 4-1]. Section 8.3.3 of that book treats the control of radar cross section of bodies by impedance loading. To quote, *"In essence this technique consists of loading the body surface with distributed or lumped impedances. As a design problem, the question arises as to what values of impedance should be used, and where should the loading be placed in order to achieve the desired cross-section control."* No general solution to this problem is given in the book, but a number of particular, simple bodies are treated, and the general principles are apparent.

Clearly the Soviet Union or another nation could make great progress in reducing the HF cross section of its cruise missiles, by relatively straightforward development from these principles. The technology required appears to be modest. The possibility of such cross-section reduction poses a substantial risk for an OTH that is supposed to detect cruise missiles. The counter by the OTH is frequency diversity, in the form of frequency hopping, or band-spanning (not necessarily band-filling) signals. However, even the

maximum possible OTH bandwidths may not be able to obviate cross-section reduction completely, particularly at night.

Let us present the principles by way of a simple example. Take a test body to be a metal cylinder of length $2h = 5$m and a diameter $2a = 0.5$m. This is a good match to the body of a cruise missile, though some will be a little longer. The first resonance lies at a wavelength $\lambda = 2 \cdot \text{length} = 4h =$ 10m, or a frequency $f = 30$MHz. The radar cross section at resonance is $\sigma \approx \lambda^2$. For radar frequencies far below the first resonance, in the Rayleigh region, the cross section drops like λ^{-4}. The lower the frequency, the *easier* the cross-section control should be.

The cross section can be controlled, for example, by electrically cutting the cylinder in half at its waist, and connecting the halves with an impedance box Z_L (Figure 4-1, from Reference 4-1). The cross section at a given frequency will depend on the chosen value of Z_L, and can be minimized either theoretically or empirically upon varying Z_L. Figure 4-2 shows cross-section plots at $f = 26$MHz for such a body. The cross section is decreased more than 30 dB by the optimal choice of Z_L.

The impedance has both resistive and reactive parts; at a single frequency it can be realized by passive components. The optimal impedance depends on frequency (Figure 4-3). To work at several different frequencies at different times, a simple switch could be implemented. To work at different frequencies at the *same* time, or to work over a substantial bandwidth, the simple impedance would have to be replaced by an appropriate filter, which in general would have to contain active components. The optimal filter can

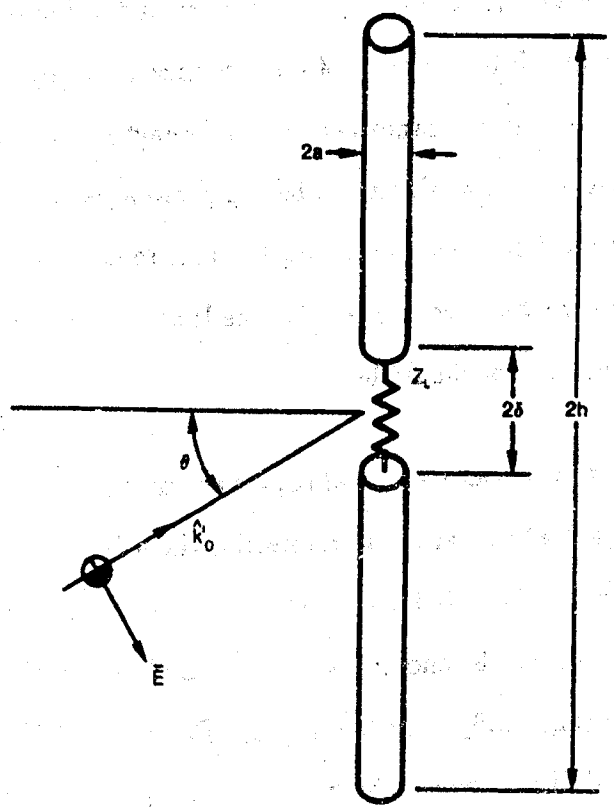

Figure 4-1. A thin center-loaded cylinder. Source: Reference 4-1.

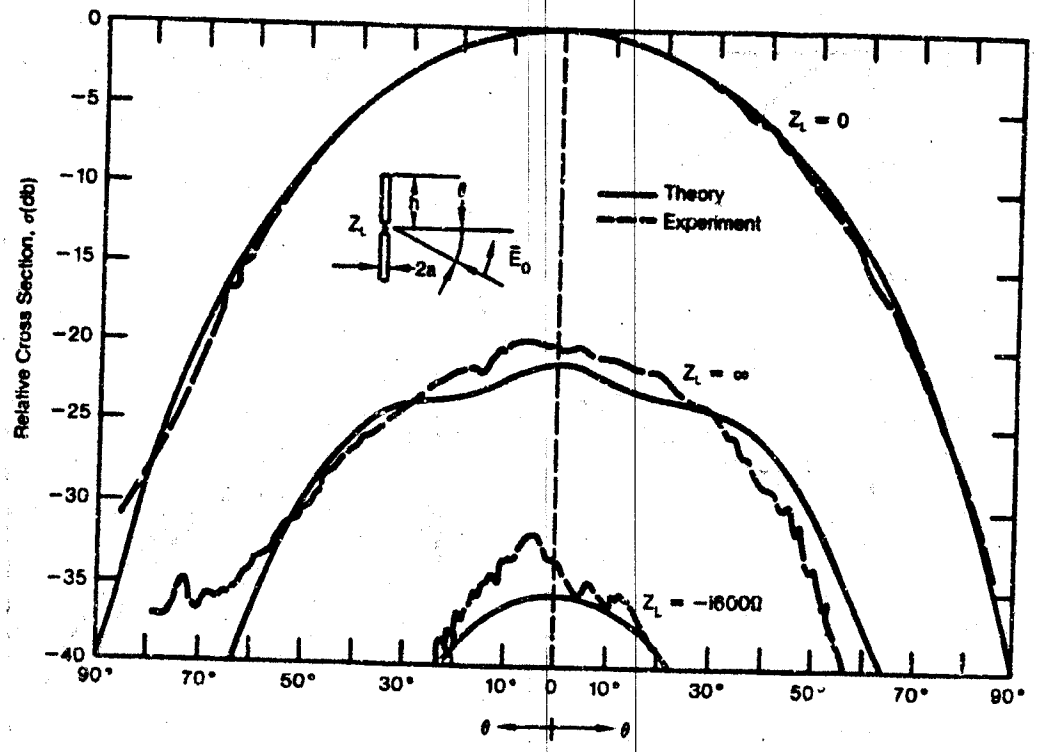

Figure 4-2. Experimental and theoretical relative backscatter cross-sections versus the angle of incidence for thin, centrally loaded cylinders with several values of load, $h = 0.215\lambda_0$, $a = 0.0173\lambda_0$. Source: Reference 4-2.

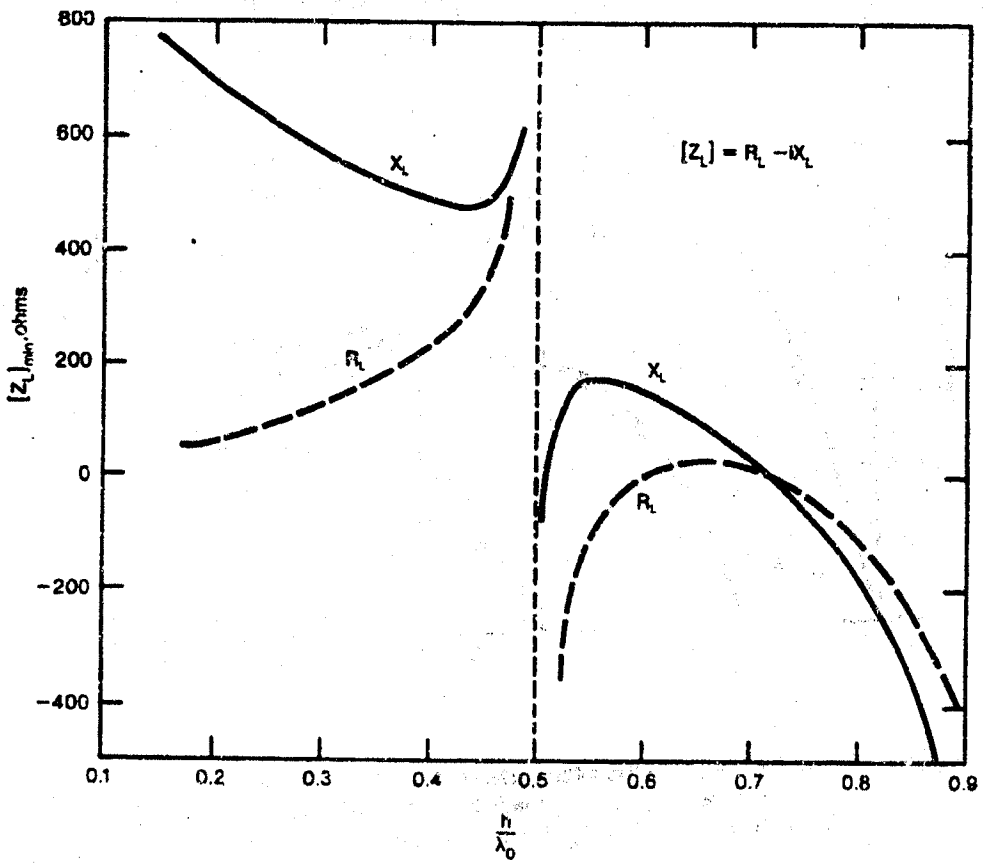

Figure 4-3. The load impedance giving zero normal-incidence backscatter for a centrally loaded cylinder with $a = 0.0173\lambda_0$, versus the cylinder half-length in wavelengths. Source: Reference 4-2.

be expected to be unrealizable over all frequencies, but straightforward engineering practice should lead to filters working over, say, 10% bandwidth in the HF. Thus, frequency diversity on the part of an illuminating OTH seems not very hard to counter.

Cutting the cruise missile in half is not necessary. The body can be loaded by impedances attached at a variety of places. Figure 4-4, again from the *Radar Cross Section Handbook*, shows cross-section reduction (at a much higher, hence much harder) frequency on a thin body using a small loaded stub at one end.

What about more complicated shapes? In particular, what about the wings and tail on a cruise missile? Here, the fact that one can work in the Rayleigh regime is of decisive importance. The electric dipole susceptibility of any body, no matter how complicated, can be measured by three principal susceptibilities, and can therefore be cancelled by only 3 appropriately located loading impedances. If significant (it probably will be insignificant), the magnetic dipole susceptibility can be cancelled by 3 more. Therefore, the dipole contribution to the radar return can certainly be cancelled by 6 loaded antennas; 3 will probably suffice. Cancelling the dipole contribution alone can reduce the cross section by more than 20 dB everywhere below the first resonance of the body at 30MHz — not all at once, but over an instantaneous bandwidth probably exceeding 10%. Figure 4-5 illustrates this principle, showing cross-section reduction for a conducting sphere. The curve $N = 6$ corresponds to elimination of the dipole return.

We conclude that the use of OTH to detect cruise missiles is susceptible

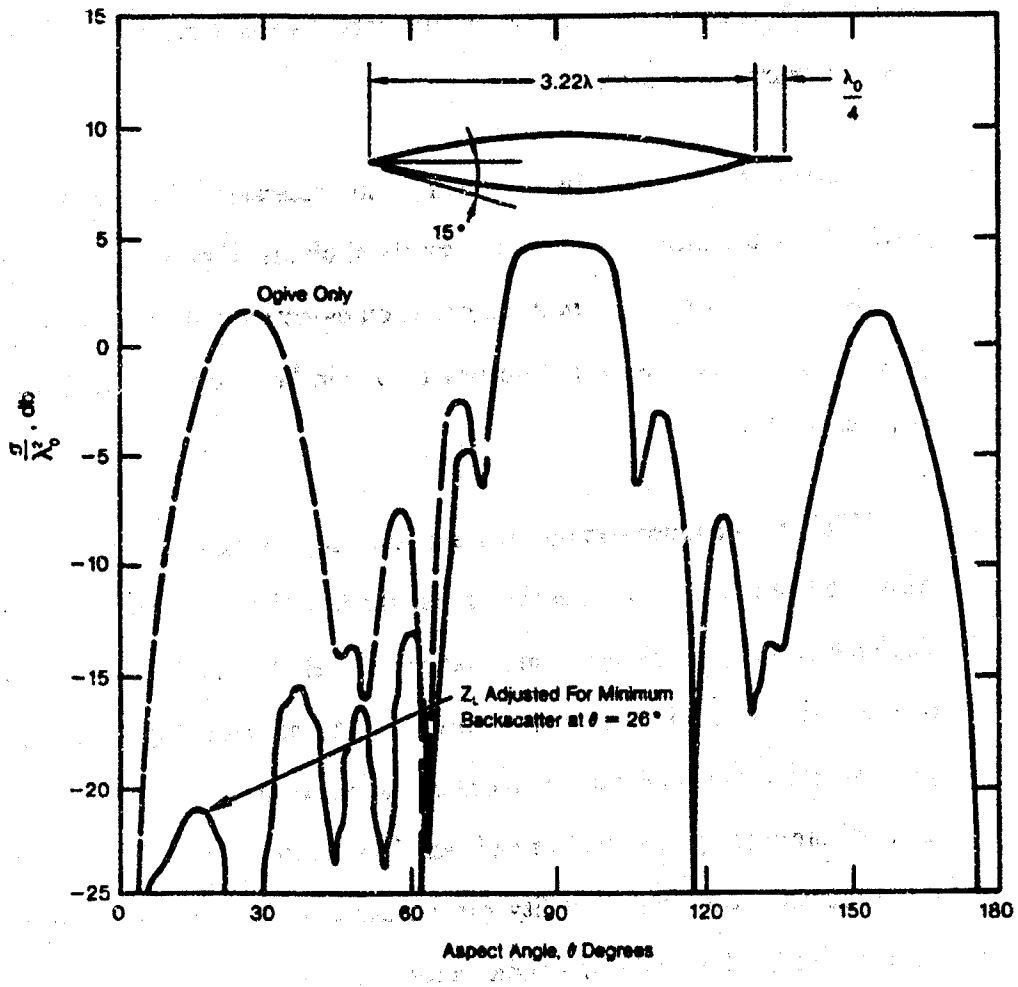

Figure 4-4. Comparison of the backscatter cross-sections of loaded and unloaded perfectly conducting ogives versus the angle of incidence. Source: Reference 4-3.

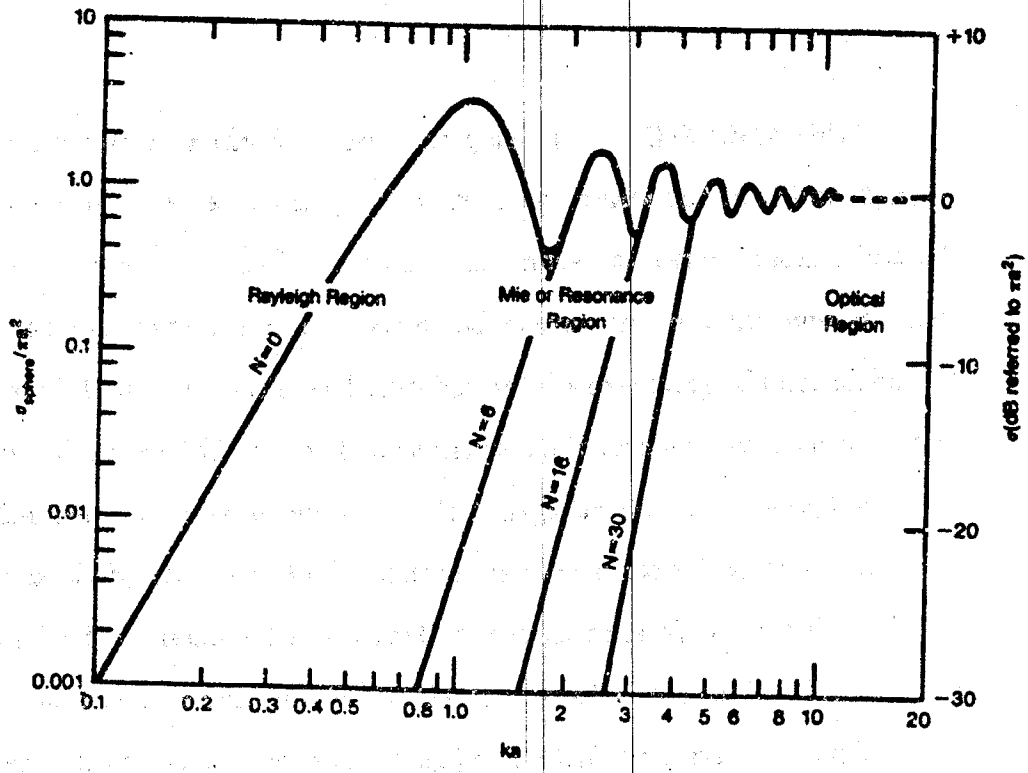

Figure 4-5. Cross-section reduction for a conducting sphere of radius a, loaded by N antennas; maximum reductions are shown.

to the possible implementation of straightfoward techniques, following from widely known principles, to reduce cross section in the HF regime.

4.2 Implications for AOTH Performance Requirements

Within ADI, OTH will probably never be 100% effective, particularly at night and at certain seasons of the year. Use of low-observable technology for cruise missiles serves to re-emphasize this point. The overall ADI surveillance system will therefore have to be viewed as a combination of sensors, including AOTH, ground-based and airborne line-of-sight radars, infrared, etc. The costs and benefits of an expensive and very ambitious AOTH system must then be traded off against the costs and benefits of other ADI components, including complementary sensors. To do this trade-off, the community will have to do some clearer thinking about the missions of AOTH within ADI: the required reliability of AOTH will be different if it is meant to discourage a preemptive first strike (i.e., to function as a deterrent), than if it is meant as part of a comprehensive active air-defense system. Unless and until the *active* components of an air defense system are built, there is not a compelling reason to have a 100% effective surveillance and tracking capability. On the other hand, to be minimally useful even in a deterrent mode, an AOTH system must be above a reasonable threshold in capability against low-observable cruise missiles, since these are a modest-cost responsive threat.

REFERENCES

4-1. *Radar Cross Section Handbook*, Vol. 2, edited by G. T. Ruck (Plenum, N.Y., 1970).

4-2. Chen K. M., and V. V. Liepa, "The Minimization of the Radar Cross Section of a Cylinder by Central Loading," Univ. of Michigan Radiation Laboratory, Report No. 5548-1-T (April 1964).

4-3. Hanson, W. P., Jr., "Backscatter Reduction of Long Thin Bodies by Impedence Loading," in *The Modification of Electromagnetic Scattering Cross Sections in the Resonant Region - A Symposium Record*, Vol. 1, edited by J. K. Schindler and R. B. Mack (Air Force Cambridge Research Laboratory, AFCRL-64-727, September 1964).

DISTRIBUTION LIST

CMDR & Program Executive Officer
U S Army/CSSD-ZA
Strategic Defense Command
PO Box 15280
Arlington, VA 22215-0150

Mr John M Bachkosky
Deputy DDR&E
The Pentagon
Room 3E114
Washington, DC 20301

(b)(3):50 USC §403(g) Section 6,(b)(3):50 USC §403-3(c)(7)
Central Intelligence Agency
Washington, DC 20505

Dr Arthur E Bisson
DASWD (OASN/RD&A)
The Pentagon
Room 5C675
Washington, DC 20350-1000

Dr Albert Brandenstein
Chief Scientist
Office of Nat'l Drug Control Policy
Executive Office of the President
Washington, DC 20500

Mr. Edward Brown
Assistant Director
DARPA/NMRO
3701 North Fairfax Drive
Arlington, VA 22203

Dr H Lee Buchanan, I I I
Director
DARPA/DSO
3701 North Fairfax Drive
Arlington, VA 22203-1714

Dr Curtis G Callan Jr
Physics Department
PO Box 708
Princeton University
Princeton, NJ 08544

Dr Kenneth M Case
1429 Calle Altura
La Jolla, CA 92037

(b)(3):50 USC §403(g) Section 6,(b)(3):50 USC §403-3(c)(7)
Central Intelligence Agency
Washington, DC 20505

Brig Gen Stephen P Condon
Deputy Assistant Secretary
Management Policy &
Program Integration
The Pentagon, Room 4E969
Washington, DC 20330-1000

Ambassador Henry F Cooper
Director/SDIO-D
Room 1E1081
The Pentagon
Washington, DC 20301-7100

Dr John M Cornwall
Department of Physics
University of California/Los Angeles
Los Angeles, CA 90024

D A R P A Library
3701 North Fairfax Drive
Arlington, VA 22209-2308

D T I C [2]
Cameron Station
Alexandria, VA 22314

Mr John Darrah
Senior Scientist and Technical Advisor
HQAF SPACOM/CN
Peterson AFB, CO 80914-5001

Dr Gary L Denman
Director
DARPA/DIRO
3701 North Fairfax Drive
Arlington, VA 22203-1714

DISTRIBUTION LIST

Dr Patrick N Diamond
6365 Cascade Street
San Diego, CA 92122

Dr Nancy Dowdy
USACDA
320 21st Street NW
Washington, DC 20451

Dr Sidney D Drell
Mail Bin 80
PO Box 4349
Stanford, CA 94309

Dr Douglas M Eardley
618 Miramonte Drive
Santa Barbara, CA 93109

Mr John N Entzminger
Chief, Advance Technology
DARPA/ASTO
3701 North Fairfax Drive
Arlington, VA 22203-1714

Capt Kirk Evans
Director Undersea Warfare
Space & Naval Warfare Sys Cmd
Code PD-80
Department of the Navy
Washington, DC 20363-5100

Dr Stanley M Flatte
678 Spring Street
Santa Cruz, CA 95060

Dr S William Gouse
Sr Vice President and
General Manager
The MITRE Corporation
Mail Stop Z605
7525 Colshire Drive
McLean, VA 22102

Col Randall Gressang
DARPA/DIRO
3701 North Fairfax Drive
Arlington, VA 22203-1714

Mr. Thomas H Handel
Office of Naval Intelligence
The Pentagon
Room 5D660
Washington, DC 20350-2000

Maj Gen Donald G Hard
Director of Space and SDI Programs
Code SAF/AQS
The Pentagon
Washington, DC 20330-1000

Dr Robert G Henderson
Director
JASON Program Office
The MITRE Corporation
7525 Colshire Drive
Mailstop Z561
McLean, VA 22102

Dr Barry Horowitz
President and Chief Exec Officer
The MITRE Corporation
202 Burlington Road
Bedford, MA 01730-1420

Dr William E Howard III [2]
Director of Advanced Concepts
& Systems Design
The Pentagon Room 3E480
Washington, DC 20301-0103

Dr Gerald J Iafrate
U S Army Research Office
PO Box 12211
4330 South Miami Boulevard
Research Triangle NC 27709-2211

DISTRIBUTION LIST

JASON Library [5]
The MITRE Corporation
Mail Stop W002
7525 Colshire Drive
McLean, VA 22102

Dr George Jordy [25]
Director for Program Analysis
U S Department of Energy
ER30
OER
Washington, DC 20585

Dr O' Dean P Judd
Los Alamos National Lab
Mail Stop A-110
Los Alamos, NM 87545

Dr Bobby R Junker
Office of Naval Research
Code 412
800 North Quincy Street
Arlington, VA 22217

Dr Gordon J Mac Donald
UCSD/0518
9500 Gilman Drive
La Jolla, CA 92093-0518

Mr Robert Madden [2]
Department of Defense
National Security Agency
Attn R-9 (Mr. Madden)
Ft George G Meade, MD 20755-6000

Dr Arthur F Manfredi Jr [10]
OSWR
Central Intelligence Agency
Washington, DC 20505

Mr Joe Martin
Director
OUSD(A)/TWP/NW&M
Room 3D1048
The Pentagon
Washington, DC 20301

Dr Claire E Max
617 Grizzly Peak Boulevard
Berkeley, CA 94708

Mr Ronald Murphy
DARPA/ASTO
3701 North Fairfax Drive
Arlington, VA 22203-1714

Dr Julian C Nall
Institute for Defense Analyses
1801 North Beauregard Street
Alexandria, VA 22311

(b)(3):50 USC §403(g) Section 6,(b)(3):50 USC §403-3(c)(7)
Central Intelligence Agency
Washington, DC 20505

Dr Peter G Pappas
Chief Scientist
U S Army Strategic Defense Command
PO Box 15280
Arlington, VA 22215-0280

Dr Ari Patrinos
Director
Environmental Sciences Division
ER74/GTN
US Department of Energy
Washington, DC 20585

Dr Francis W Perkins Jr
Plasma Physics Laboratory
PO Box 451
Princeton University
Princeton, NJ 08543

DISTRIBUTION LIST

Dr Allen M Peterson
14846 Manuela Avenue
Los Altos Hills, CA 94022

Dr Bruce Pierce
USD(A)D S
Room 3D136
The Pentagon
Washington, DC 20301-3090

Mr John Rausch [2]
Division Head 06 Department
NAVOPINTCEN
4301 Suitland Road
Washington, DC 20390

Records Resource
The MITRE Corporation
Mailstop W115
7525 Colshire Drive
McLean, VA 22102

Dr Fred E Saalfeld
Director
Office of Naval Research
800 North Quincy Street
Arlington, VA 22217-5000

Dr John Schuster
Technical Director of Submarine
and SSBN Security Program
Department of the Navy OP-02T
The Pentagon Room 4D534
Washington, DC 20350-2000

Dr Barbara Seiders
Chief of Research
Office of Chief Science Advisor
Arms Control & Disarmament Agency
320 21st Street NW
Washington, DC 20451

Dr Philip A Selwyn [2]
Director
Office of Naval Technology
Room 907
800 North Quincy Street
Arlington, VA 22217-5000

Dr Jeremiah D Sullivan
604 Burkwood Court, East
Urbana, IL 61801

Superintendent
Code 1424
Attn Documents Librarian
Naval Postgraduate School
Monterey, CA 93943

Dr George W Ullrich [3]
Deputy Director
Defense Nuclear Agency
6801 Telegraph Road
Alexandria, VA 22310

Ms Michelle Van Cleave
Asst Dir/National Security Affairs
Office/Science and Technology Policy
New Executive Office Building
17th and Pennsylvania Avenue
Washington, DC 20506

Dr John F Vesecky
University of Michigan
1424A Space Research Bldg
Ann Arbor, MI 48109-2143

Mr Richard Vitali
Director of Corporate Laboratory
US Army Laboratory Command
2800 Powder Mill Road
Adelphi, MD 20783-1145

DISTRIBUTION LIST

Dr Edward C Whitman
Dep Assistant Secretary of the Navy
C3I Electronic Warfare & Space
Department of the Navy
The Pentagon 4D745
Washington, DC 20350-5000

Mr Donald J Yockey
U/Secretary of Defense For Acquisition
The Pentagon Room 3E9333
Washington, DC 20301-3000

(b)(3):50 USC §403(g) Section 6,(b)(3):50 USC §403-3(c)(7)
Central Intelligence Agency
Washington, DC 20505

Mr Charles A Zraket
Trustee
The MITRE Corporation
Mail Stop A130
202 Burlington Road
Bedford, MA 01730

[This page is intentionally left blank.]